

# IRE TRANSACTIONS



## ON BROADCASTING

Volume BC-6  
Follows PGBC-14

MARCH, 1960

Number 1

### TABLE OF CONTENTS

A Resonant Coaxial-Stub as an Automatic Equalizer . . . . .	G. V. Rao
Television Antenna System Measurements Based on Pulse Techniques . . .	D. W. Peterson
New Equipment for Measuring Envelope Delay . . . . .	E. N. Luddy
Reactivation of Image Orthicons under Low Temperatures . . . . .	B. Wolfe
Some Color Slide and Color Television Experiments Using the Land Technique	W. L. Hughes
Design and Performance Measurements on a New Anti-Fade Antenna for Radio Station WOAI . . . . .	C. L. Jeffers and S. W. Kershner

PUBLISHED BY THE  
PROFESSIONAL GROUP ON BROADCASTING

## **IRE PROFESSIONAL GROUP ON BROADCASTING**

The Professional Group on Broadcasting is an organization, within the framework of the IRE, of members with principal professional interest in Broadcasting. All members of the IRE are eligible for membership in the Group and will receive all Group publications upon payment of prescribed fee.

Annual Fee: \$2.00

### **Administrative Committee**

**GEORGE E. HAGERTY, *Chairman***

**E. W. ALLAN, *Vice-Chairman***

**J. W. WENTWORTH, *Secretary-Treasurer***

**J. L. BERRYHILL**

**W. L. HUGHES**

**R. J. ROCKWELL**

**F. J. BIAS**

**R. S. KIRBY**

**R. W. RODGERS**

**R. F. GUY**

**O. L. PRESTHOLDT**

**J. G. ROUNTREE**

**H. T. HEAD**

**L. E. RAWLS**

**GEORGE TOWN**

### *Ex-Officio*

**CLURE H. OWEN**

### **IRE TRANSACTIONS®**

#### **on Broadcasting**

Published by the Institute of Radio Engineers, Inc., for the Professional Group on Broadcasting at 1 East 79th Street, New York 21, New York. Responsibility for the contents rests upon the authors, and not upon the IRE, the Group or its members. Individual copies available for sale to IRE-PGBC members at \$0.80, to IRE members at \$1.20 and to nonmembers at \$2.40

---

COPYRIGHT ©1960 — THE INSTITUTE OF RADIO ENGINEERS, INC.

All rights, including translation, are reserved by the IRE. Requests for republication privileges should be addressed to the Institute of Radio Engineers, 1 East 79th Street, New York 21, N. Y.

PRINTED IN THE U.S.A.

A RESONANT COAXIAL-STUB  
AS AN AUTOMATIC EQUALIZER

G. V. Rao  
Radio Corporation of America  
Camden 2, N. J.

Abstract

This paper describes a novel application of a resonant coaxial-stub which is very short in comparison with the shorter wavelengths in the video spectrum. As far as the principle of operation is concerned, the designation "resonant reactance stub" appears to be an appropriate term for the short piece of the coaxial cable used in this application. The stub provides automatic equalization at the input of a video circuit which presents a changing capacitance from time to time as a result of the incidence of additional video loops with appreciable input-capacity.

The coaxial-stub has some interesting applications in video work, (1) as an automatic equalizer in color and monochrome video switching systems, (2) for high-frequency equalization of the video distribution cables used in television studios and (3) as an input high-frequency matching device in video distribution amplifier systems.

Introduction

It is well known that a coaxial cable, as a passive transmission line network with distributed constants, produces resonant effects due to combination of incident and reflected waves when it is terminated by a load impedance that is appreciably different from its characteristic impedance. The voltage and current distributions from the receiving end onward depend upon the exact nature of the actual terminating impedance used, but always follow cyclic variations of maxima and minima, as a function of an exact multiple of a quarter-wavelength at the frequency of interest (Fig. 2). A progressive lag of  $360^\circ$  per wavelength takes place during the transit from the generator to the load, mostly around the voltage and current minima. By confining the attention to a quarter-wave resonant line, we can say that the resonant stub acts like a step-up transformer at the corresponding frequency when it is terminated by (1) an open-circuit or (2) a high resistance or (3) a capacitive reactance or (4) a capacitive reactance with a resistive-shunt. As an extension to the above statement, we can say that a fixed length of a short resonant stub will have a progressively diminishing step-up ratio as the transmitting frequency is lowered. The impedance of this line in the vicinity of the resonant frequency varies according to exactly the same law as that applicable to the impedance of a series resonant circuit.

If the above resonant stub is further shortened to a small fraction of  $\lambda/4$ , the sending-end impedance primarily becomes reactive with a capacitive reactance and a low power factor, and is proportional to the characteristic impedance, and varies cyclically with length. The  $Q$  varies with line proportions and frequency according to the same law for both the  $\lambda/4$  resonant line and the reactance stub. In general, the reactance presented by the "resonant reactance stub" (as the coaxial-stub under consideration is termed) enables a very high selectivity, and therefore the lowest loss.

General Equalizer Action

Figure 3 gives an enlarged view of the voltage distribution characteristics for a resonant reactance stub, with an open-circuit at the receiving end, at three frequencies of interest in the video pass-band. If the stub-length is chosen, for clarity sake, say a fraction like  $\lambda/16$  at 6 Mc (the actual length may be of the order of a quarter of this fraction), a sending-end voltage  $E_{S1}$  of the voltage distribution curve at 6 Mc is stepped up to  $E_R$  at the receiving end. The same stub can then be considered as an equivalent length  $\lambda/32$  at 3 Mc. In this case, the step-up function involved produces a slope of  $\tan \theta_2$  which is much smaller than  $\tan \theta_1$  for the 6 Mc case; and so the process extends down to the lowest frequency of interest. The desired video pass-band and the actual length of the short stub chosen determines the highest video frequency at which the boost is effectively maximum.

If under prevailing conditions at the input of a video circuit, there is at the outset a gradual fall-off of the output frequency response at 6, 3, and 1.5 Mc from the normal output level indicated by  $d$  to the levels indicated by  $a$ ,  $b$  and  $c$  respectively, it is clear from the graphic representation of the slopes obtained from the three voltage distribution characteristics and the short resonant stub (Figs. 3 and 4.2) that a process of equalization takes place to maintain a flat response characteristic at the receiving end along the reference level  $d$  at the three frequencies under consideration (and the whole pass-band of interest), provided the optimum length of the stub and the extent of deterioration in the original high frequency response match one another. The optimum length for the

requisite pass-band is best determined by experiment, since an analytical computation with the stray inductive and capacitive variables involved in practice will prove to be far too complex.

It is seen from Fig. 2.5 that a comparatively high resistance termination is fairly effective in reducing the slope of the resonant characteristic of a transmission line. The result is something analogous to the effect of a damping resistance in a series resonant circuit. Therefore the stub-termination at the receiving-end (whether it should be left open-circuited or terminated by an appropriate high resistance) is best decided in the light of the actual requirements of a specific case of application.

#### Process of Automatic Equalization

The performance of the resonant reactance stub at the video channel input of, say, a multi-output switching system is a further development to the above general equalizer action. In this application, the stub is required to maintain a satisfactory system response characteristic automatically, while it is associated with a changing capacitive load on the input video bus, as the switching manipulation takes place for various number of output conditions from time to time.

Incidentally, at the present state of the art, a video switching system is "peaked" for the worst case of capacitive load on the input bus, and the capacity of each output video bus is replaced by means of a relay in the release position of each output by an equivalent capacitor. This capacitance then makes a lumped constant parameter for a specially designed constant-K LC transmission network along the input video bus. The actual method of equalization is in practice very cumbersome indeed. With the resonant reactance stub, the subtle process of automatic equalization takes place in the following manner.

When a transmission line is terminated by a capacitive reactance, that is equal in magnitude to the characteristic impedance of the line at the frequency of interest, the r.m.s. voltage and current distributions along the line take the form shown in Fig. 2.6. The distribution is essentially of the same character as that of a transmission line with an open-circuit at the receiving end, except that the distribution curves exhibit a marked tendency to a shift-in-toto toward the receiving end. And it can be shown by plotting the voltage distribution curves for various capacitive loads that the shift referred to increases as the capacitive reactance is reduced. Since the sending-end impedance of a short resonant reactance stub as shown in Fig. 2.3 is extremely high towards the receiving end, the capacitive

reactance at the receiving end is all that matters. But the capacitive reactance is inversely proportional to frequency. Hence it is seen that the shift-in-toto of the voltage distribution curves in Fig. 4.1 increases with frequency for a preselected capacitive termination. That is, as far as the short length of the stub is concerned, the slope of response obtainable with a capacitive load is one of a higher degree. Thus, where a higher slope for the high frequency boost is desired, the capacitive termination presents an effective means, provided the resultant envelope delay distortion in the actual pass-band is negligibly minute. If a small amount of envelope delay distortion is originally present, due to a rapid fall-off of h.f. response the reactance stub will naturally improve the situation, by cancelling part of the original distortion, while it produces the increased boost at the higher frequencies in the pass-band by virtue of the capacitive load, which by itself is otherwise responsible for the original fall-off.

For a clear understanding, the operation of the reactance stub as an automatic equalizer is graphically explained by referring to its actual application in a complex video switching system. Referring to Fig. 5.1, if the capacitive load is halved by the output switching manipulation, the capacitive reactance at each frequency under consideration is doubled in magnitude and the shifts-in-toto of the voltage distribution curves away from  $\lambda/4$  positions are progressively reduced. It is clear from Fig. 5 that the three voltage distribution curves at 6, 3 and 1.5 Mc shift automatically to give reduced slopes for the voltages obtainable at the receiving-end of the stub in the new situation. The new order of the exponential voltage step-up with increasing frequency gives a lower overall slope for the various frequency components in the video spectrum, (Fig. 5.2) and this is naturally compatible with the effect of a reduced capacitive load due to the stacking of a less number of output video buses across the line termination. A high resistance across the receiving end of the reactance stub merely provides a kind of fine control for the slope of a fixed length of the stub at each video channel input. How effective is the process of automatic equalization, that takes place to maintain a flat video frequency response characteristic under two switching conditions, viz. two outputs and four outputs across a video channel in a complex 13-channel video switching system, is shown in Fig. 6. Response characteristics a' and b', reproduced in Fig. 6, indicate the exact nature of the results obtained in the actual switching application. It may be noted that the input capacities involved are of the order of as much as 200 to 400  $\mu\text{f}$ .

## Practical Examples

1. In the case of the above 18-channel switching system, the channels are divided into three 6-ch. sections in order to compensate the long connecting leads used for the output video buses in the lower sections by means of small peaking coils in the upper sections. These coils and lead-lengths produce a semblance of "stub" effect over and above the desired action of the chosen two-foot resonant reactance stub for a particular channel. As a countermeasure to the undesirable "stub" effects, the slope of the reactance stub (of a fixed length) at each channel input is gradually lowered from the top to the bottom by terminating each coaxial-stub with a high resistance that diminishes in value from the top to the bottom. The coils are heavily damped to prevent their electrical lengths from interfering with the smooth process of automatic equalization accomplished by the chosen stubs under the various output switching conditions. In fact, a small coil with a high Q can approximately perform like a stub in much simpler applications on the same principle. A thin copper strip is preferred for the various video connections so as to obtain maximum discontinuity for the undesirable "stub" effects. An 18-channel/4-output video switcher, was found to give after the above custom-modification an overall response performance within 1% at 3.6 Mc, and within 2 to 3% at 6 Mc under the worst switching conditions, and better performance towards the high frequency end (beyond 6 Mc) under less severe switching conditions for all the 18 channels. Without the resonant reactance stub, the normal output was down by 7 to 10% at 3.6 Mc, and 20 to 25% at 5.5 Mc under the worst switching conditions (with 4 outputs "ON") for some of the channels.

As compared to other conventional methods, the experimental design with a reactance stub is very simple, and no additional video relay contacts are involved. The variable-slope technique used for the various channels minimizes the delay connected with the longer path-lengths, and makes the phase-shift negligible between the various channels and the various outputs. And problems of cross-talk are minimized by eliminating the use of coils etc. along the video input bus for each channel.

2. A coaxial-stub (RG-59/U), 18" long, open-circuited at the receiving-end (with line termination at the sending-end of the stub), was found to equalize a length of about 45 feet of RG-59/U coaxial cable right up to 10 Mc. The short reactance stub by itself has negligible insertion loss. It is normally impractical to use equalizer networks with insertion loss for short lengths of distribution cables; nor is it desirable to peak a piece of video equipment for the h.f. losses in the preceding distribution cable, which might be changed over by remote switching from time to time. The resonant

reactance stub is thus a simple solution for individually equalizing studio distribution cables (Fig. 8).

3. The coaxial-stub serves, in particular, as an excellent input high frequency matching device when a large number of distribution amplifier modules (with single output connections) are looped across a common video input. A flat frequency characteristic is maintained at the output of each DA module right to 8 Mc or so, irrespective of the total input capacity contributed by the DA modules "IN" at any instant. The optimum length of the coaxial-stub is, as explained, determined by (1) the desired cut-off frequency and (2) the total capacity due to the maximum number of DA modules allowed (Fig. 9).

The resonant reactance stub, in general, allows the insertion of one or more additional video units at the termination of a video distribution cable without any noticeable impairment to the frequency response of the respective outputs. The coaxial reactance stub is hence a very useful and handy device in installation work connected with television studios.

## Conclusion

The basic theory of the reactance stub is extensively dealt with in literature. As far as the practice is concerned, the simple resonant reactance stub provides a very attractive method for accomplishing automatic equalization in video systems which present the problem of a changing capacitive load from one instant to another. Usual equalizer network design does not offer any scope in this particular direction. A solution to problems of this kind is of vital importance especially in color television systems, and the simple experimental technique involved in the design of a short coaxial stub, with a given characteristic impedance, for a single parameter, viz. length (and a terminating high resistance in some cases) appears to present a reliable and effective answer.

## Acknowledgment

The author is indebted to Mr. J. W. Wentworth, TV Terminal Engineering, RCA, for his permission to publish this paper, and his encouragement during the progress of the development work connected with this application.

## Appendix

### Theoretical Interpretation

A coaxial cable is basically a passive transmission line network in which (1) the physical dimensions are comparable to the wavelengths of the currents flowing and (2) the series resistance and inductance of the conductor, and the shunt capacitance and leakage between conductor and screening are considered as

distributed along the length of the cable.

It is well known that a transmission line can be operated as a resonant or non-resonant device in accordance with the choice of load impedance at the receiving end, as compared to the iterative or characteristic impedance of the line.

If the receiving load  $Z_L$  is a pure resistance equal to the characteristic impedance  $Z_0$ , the line is non-resonant since no reflection occurs, and the voltage and current distributions follow an exponential law as shown in Figure 1, allowing transmission of power at unity power factor.

$$Z_0 = \frac{R \neq j\omega L}{G \neq j\omega C}$$

where R and G are resistance and conductance (or leakage) per unit length of line. At radio frequencies,  $\omega$  is so large that R and G can be neglected.

$$Z_0 = \frac{L}{C}$$

The actual characteristic impedance is determined by the physical construction of the transmission line, and in the case of the coaxial line,

$$Z_0 = \sqrt{\epsilon} \frac{138 \text{ Log}_{10} \frac{b}{a}}$$

where  $\epsilon$  is the dielectric constant of the insulation material filling the line, 'b' is the inside diameter of outer screening and 'a' is the outside diameter of the inner conductor. The resistance R is determined largely by the skin-effect and is given by:

$$R = 41.6 \sqrt{f} \left( \frac{1}{a} \neq \frac{1}{b} \right) 10^{-9} \text{ ohms/cm.}$$

However, if the load impedance is appreciably different from the said characteristic impedance, resonance effects are produced due to combination of incident and reflected waves, and the voltage and current distributions at the frequency of interest follow, as in Figure 2, cyclic variations of maxima and minima as a function of an exact multiple of a quarter wavelength from the receiving end. The reflection coefficient of the standing-wave pattern so created at that frequency is determined by the ratio of  $Z_L/Z_0$  as given by the equation:

$$\text{Reflection Coefficient at receiving end, } \rho = \frac{(Z_L/Z_0) - 1}{(Z_L/Z_0) \neq 1}$$

In travelling from generator to load, there is a progressive lag of  $360^\circ$  (or  $2\pi$  radians) per wavelength; but instead of taking place at a uniform rate (as in the case of a non-resonant line), most of the phase-shift takes place around the voltage and current

minima as shown in Figure 2. The ratio of maxima and minima in a distribution depends on the resistance per unit length. The value of R diminishes at higher ratios.

The general expression for the sending-end impedance is given by:

$$Z_s = Z_0 \frac{(Z_0 \neq Z_L)e^{\gamma' l} - (Z_0 - Z_L)e^{-\gamma' l}}{(Z_0 \neq Z_L)e^{\gamma' l} \neq (Z_0 - Z_L)e^{-\gamma' l}}$$

where  $\gamma'$  is called the propagation constant, and is given by:

$$\gamma' = \alpha \neq j\beta,$$

$\alpha$  and  $\beta$  being the attenuation constant and the phase-shift constant respectively:

$$\alpha = \sqrt{\frac{1}{2} \sqrt{(R^2 \neq \omega^2 L^2)(G^2 \neq \omega^2 C)} \neq (RG - \omega^2 LC)}$$

$$\text{and } \beta = \sqrt{\frac{1}{2} \sqrt{(R^2 \neq \omega^2 L^2)(G^2 \neq \omega^2 C)} - (RG - \omega^2 LC)}$$

The general expression for the rms voltage is given by the equation:

$$E_x = \sqrt{A^2 e^{-2\alpha x} \neq B^2 e^{2\alpha x} / 2AB \cos(\delta_A - \delta_B - 2\beta x)}$$

and it will have maximum and minimum values along the line whenever  $B \neq 0$ , since  $\cos(\delta_A - \delta_B - 2\beta x)$  changes more rapidly than  $e^{2\alpha x}$ . When attenuation is negligible and  $A = B$  (with complete reflection, and no absorption of power), the above expression reduces to:

$$E_x = \sqrt{2A^2 - 2A^2 \cos(\delta_A - \delta_B - 2\beta x)}$$

Thus along the transmission line there are positions, where  $E_x = 2A$ , called voltage-loops and others, where  $E_x = 0$ , called voltage-nodes. In order for A to equal B,

$$e^{2\gamma' l} = \pm \frac{Z_L - Z_0}{Z_L \neq Z_0}$$

For any line, a multiple of a quarter-wavelength long, with a negligible attenuation,  $e^{2\gamma' l} = e^{jn\pi}$  where n is an integer. Hence true standing-waves will occur as shown in Figure 2 when  $Z_L = 0$  or  $Z_L = \infty$  (short-circuited and open-circuited lines, respectively).

For an open-circuit at the receiving end, the sending-end impedance,  $Z_s$  is then simplified to:

$$Z_s = E_s / I_s = \frac{E_r \cosh(\alpha \neq j\beta) l}{(E_r / Z_0) \sinh(\alpha \neq j\beta) l}$$

$$Z_s = \frac{Z_0}{\tanh(\alpha \neq j\beta) l}$$

where  $l$  is the line-length,  $E_r$  is the voltage at the receiving end, and  $(\alpha \neq j\beta)$  is the propagation constant of the line.  $\alpha$  and  $\beta$  are both

functions of frequency, and  $\beta$  is now given by:

$$\omega\sqrt{LC}$$

Voltage and current distributions for transmission circuits with 'distributed' constants are shown in Figure 2 with standing-wave conditions existing under different terminating conditions at the receiving end. Figure 2.3 and 2.4 give the characteristics for the sending-end impedance of the line corresponding to Figures 2.1 and 2.2. The power-factor passes through unity whenever either the voltage or the current is at a minimum, and stays put at nearly 90°, leading or lagging, for other conditions.

It is clear from Figures 2.3 and 2.4 that the impedance of a transmission line at the sending-end, looking towards the receiver, more or less follows the voltage distribution, being (1) very high for a voltage maxima and (2) low for a voltage minima.

Changing the frequency naturally alters the number of maxima and minima occurring in a given length of line, but it does not alter the line behavior in any way. And the distance, along the line, corresponding to a wavelength is given by the expression:

$$\frac{1}{f\sqrt{LC}}$$

The length of the resonant stub used in the present application is a mere fraction of a quarter-wavelength at the higher frequencies of interest in the video frequency spectrum. Considering a quarter-wave resonant line, to start with, for a closer investigation into the theoretical aspect of the solution, it is clear from Figure 2.1 that a quarter-wave resonant line with an open-circuited receiver (or a high resistance termination) produces a change in voltage from the sending end toward the receiving end that closely resembles that of a series resonant circuit.

$$\frac{\text{Receiving-end voltage}}{\text{Sending-end voltage}} = \frac{E_r}{E_s} = \text{step-up ratio.}$$

The quarter-wave resonant stub acts like a step-up transformer under this condition at the corresponding frequency. As the frequency is varied slightly about the resonance, the impedance of the line varies according to exactly the same law that is applicable to the impedance of a series resonant circuit. When the stub is an even number of quarter-wavelengths long, the law applicable is that which corresponds to parallel resonant circuits. The selectivity of the quarter-wave resonant line is given in terms of a selectivity factor Q by the following expression.

$$Q = \frac{2\pi Z_0}{R_c}$$

where c is the velocity of light.

For a concentric line, it can be shown that,

$$Q = 0.0839 \sqrt{f} b.H$$

where H is a function of b/a and is less than 1.

$$\text{And ratio of voltage step-up} = \frac{8Z_0 f}{R_{nc}}$$

where n is the number of quarter-wavelengths in a line. In the present case, n is equal to unity.

Since the voltage step-up ratio in the vicinity of resonance has exactly the same type of selectivity characteristic as the voltage step-up in an ordinary resonant circuit,

$$Q = \frac{2\pi Z_0}{R_c}$$

and the step-up obtainable for a quarter-wave resonant line } = \frac{8Z\_0 f}{R\_{nc}} \times \frac{R\_c}{2\pi Z\_0} Q = \frac{4}{\pi} Q

Thus the step-up obtainable with a  $\lambda/4$  resonant stub is greater than that obtained with a simple resonant circuit. Unlike ordinary resonant circuits, this step-up tends to increase with (1) frequency (as an additional advantage) and (2) higher Q obtainable with resonant lines.

The sending and receiving impedances can be shown to be related to the characteristic impedance of the quarter-wave resonant stub by the equation:

$$Z_0 = \sqrt{Z_s Z_L}$$

where  $Z_L$  is the receiving load impedance.

When a resonant line, that is open or short-circuited at the receiving end, is a fraction of a quarter-wavelength, the sending-end impedance is primarily reactive with a low power-factor. The nature of the reactance can be seen by re-arranging equation for  $Z_s$ , given by the following expression for a resonant transmission line of a length suitable to give high sending-end impedance.

$$Z_s = \frac{8Z_0^2 f}{R_{nc}}$$

Neglecting terms that are unimportant at or near resonance, the following equation may be derived from the above equation:

$$Z_s = \frac{R_c (\ell/\lambda)}{2f \sin^2 2\pi(\ell/\lambda)} - j \frac{Z_0}{\tan 2\pi(\ell/\lambda)}$$

This equation, of course, does not hold when  $\ell/\lambda$  approaches an integral number of quarter-wavelengths.

The reactance component of  $Z_s$ , from above equation, is proportional to  $Z_0$  and it varies cyclically with length. Thus the reactance can be varied by either altering  $Z_0$  or the length of the stub.

The (reactance/resistance) component of  $Z_s$  can be referred to as the selectivity-factor of the 'reactance' stub, and

$$Q = \frac{Z_0 f}{R_c} \times \frac{\sin 4\pi(l/\lambda)}{(l/\lambda)}$$

Comparing this with  $Q$  for a  $\lambda/4$  resonant line,

$$Q = \frac{2\pi Z_0 f}{R_c}$$

it is seen that  $Q$  varies with (1) line proportions and (2) frequency, according to the same law, for both the impedance of the quarter-wave resonant line and the 'reactance' stub. Also the  $Q$  of the 'reactance' stub under reference compares favorably with that of the quarter-wave resonant line.

In general, the reactance obtained by a "reactance" stub varies far more rapidly with frequency than does the ordinary reactance with lumped constants, and the line has, of course, comparatively a very high selectivity. A short-circuited stub less than a quarter-wavelength long behaves like an inductive-reactance with the lowest loss, and an open-circuited stub less than a quarter-wavelength long behaves like a capacitive reactance with the characteristics explained above. And it is in this form, the short resonant coaxial-stub is used in the present application as an automatic equalizer.

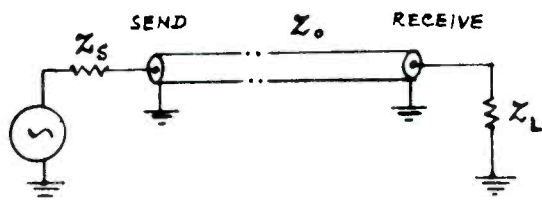


Fig. 1 - Voltage and current distribution characteristics for a (non-resonant) transmission line with normal terminations at the sending and receiving ends.

$$Z_0 = Z_s = Z_L$$

### Resonant Reactance Stub as an Automatic Equalizer

How the voltage distribution characteristics for two different capacitive loads shift in phase to give the requisite variation in slope can be shown by plotting the resonance curves for the first quarter-wavelengths at two frequencies under consideration by means of the following equation:

$$E_x = A e^{-\gamma' x} + B e^{\gamma' x}$$

where  $\gamma'$  is the propagation constant,

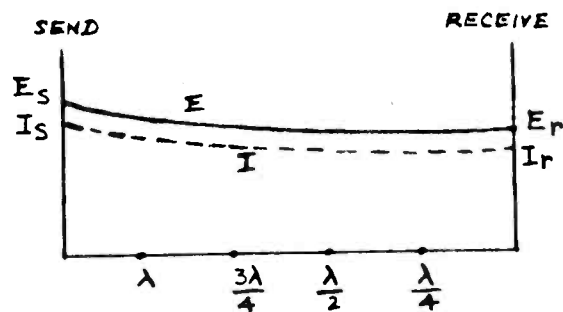
$$A = \frac{(Z_0 + Z_L) e^{\gamma' l}}{(Z_0 + Z_L) e^{\gamma' l} - (Z_0 - Z_L) e^{-\gamma' l}} \cdot E_0$$

$$\text{and } B = \frac{(Z_L - Z_0) e^{-\gamma' l}}{(Z_0 + Z_L) e^{\gamma' l} - (Z_0 - Z_L) e^{-\gamma' l}} \cdot E_0$$

$Z_0$  is the characteristic impedance of the cable;  $E_0$  is the impressed voltage; and (1)  $Z_L = X_{c.1}$  and (2)  $Z_L = X_{c.2}$  for the two characteristics. These two characteristics are employed to evaluate the slope of equalization for the length of the stub used under conditions of two different capacitive loads across the receiving end of the stub.

#### Bibliography

1. Terman, F. E.; "Resonant Lines in Radio Circuits", PP. 1046-1053; July 1934; Electrical Engineering.
2. Pender, H. and McIlwain, K.; Electrical Engineer's Handbook, Electrical Communication and Electronics, Third Edition, Section 5, PP. 3.09-3.22.



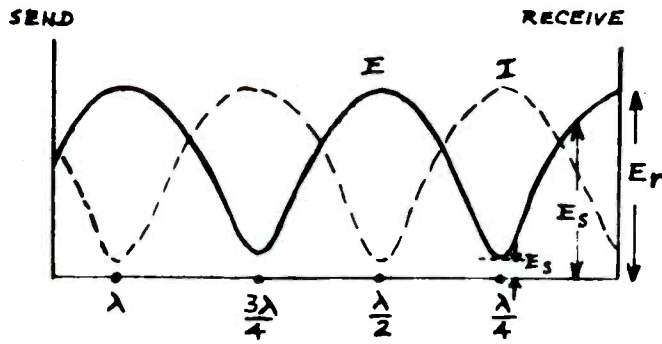


Fig. 2.1 - Voltage and current distribution characteristics for a (resonant) transmission line open-circuited at the receiving-end.

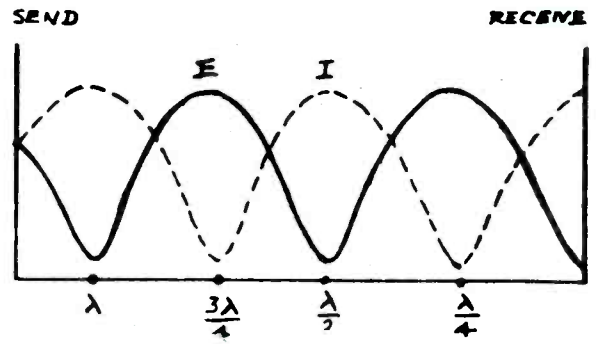


Fig. 2.2 - Voltage and current distribution characteristics for a (resonant) transmission line short-circuited at the receiving-end. (Inductive reactance termination is similar to the short-circuited case except that the waveforms are bodily shifted like those in the capacitive reactance case, shown in Fig. 2.6).

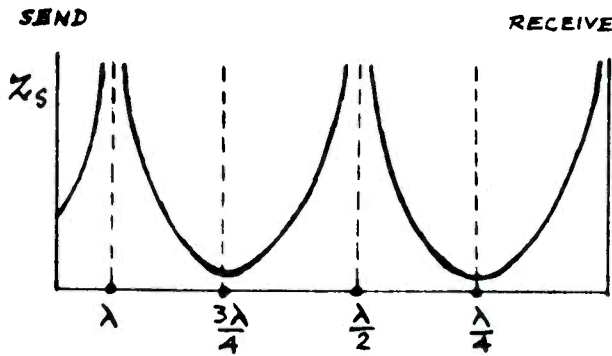


Fig. 2.3 - Change in sending-end impedance with length when the transmission line is open-circuited at the receiving-end.

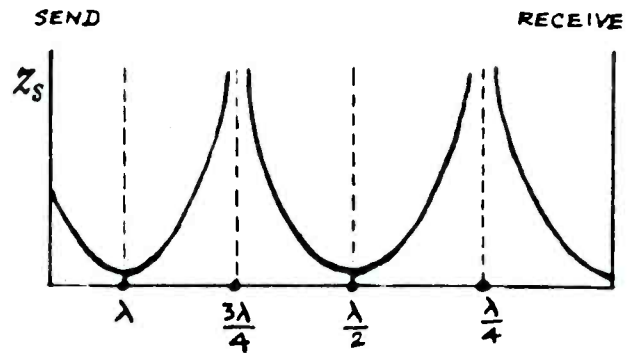


Fig. 2.4 - Change in sending-end impedance with length when the transmission line is short-circuited at the receiving-end.

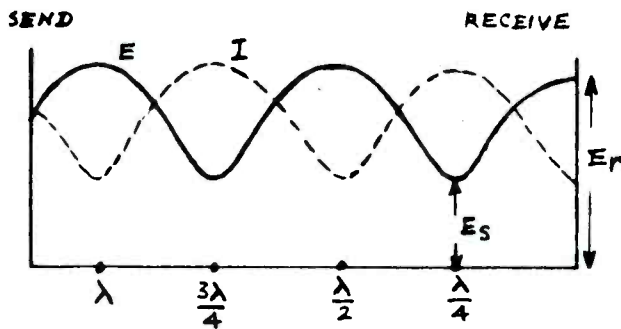


Fig. 2.5 - Voltage and current distribution characteristics for a (resonant) transmission line terminated by a resistor that is appreciably larger than the characteristic impedance of the line.

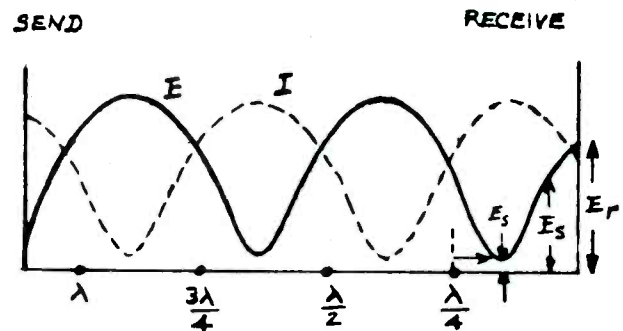


Fig. 2.6 - Voltage and current distribution characteristics for a (resonant) transmission line terminated by a capacitive reactance that is equal in magnitude to the characteristic impedance of the line.

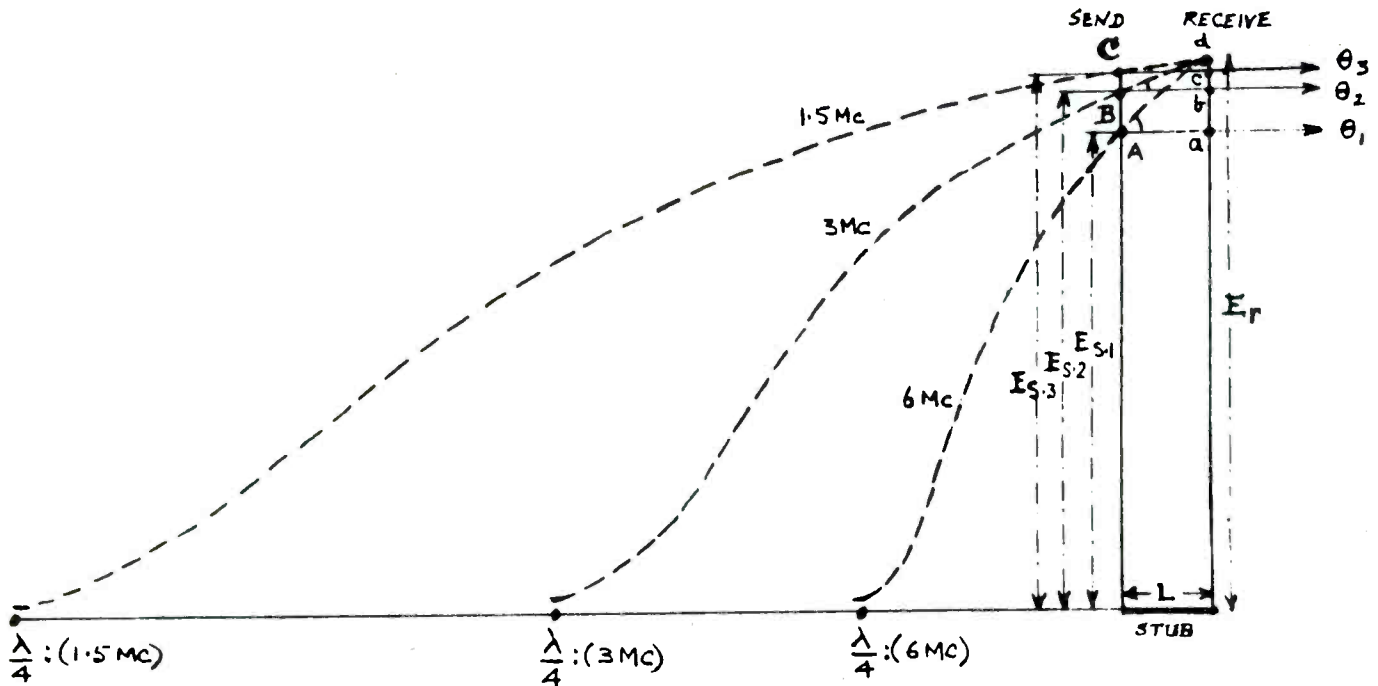


Fig. 3 - The voltage distribution characteristics of a short resonant coaxial-stub (open-circuited at the receiving-end) at 6, 3, and 1.5 Mc., depicting its performance as a general high frequency equalizer. If  $\delta_a$ ,  $\delta_b$ , and  $\delta_c$  are system attenuations at 6, 3 and 1.5 Mc. respectively, stub  $L$  equalizes their amplitude response to the desired output level  $d$  at the receiving-end. Actual stub length used: approximately  $\lambda/60$  at 6 Mc.

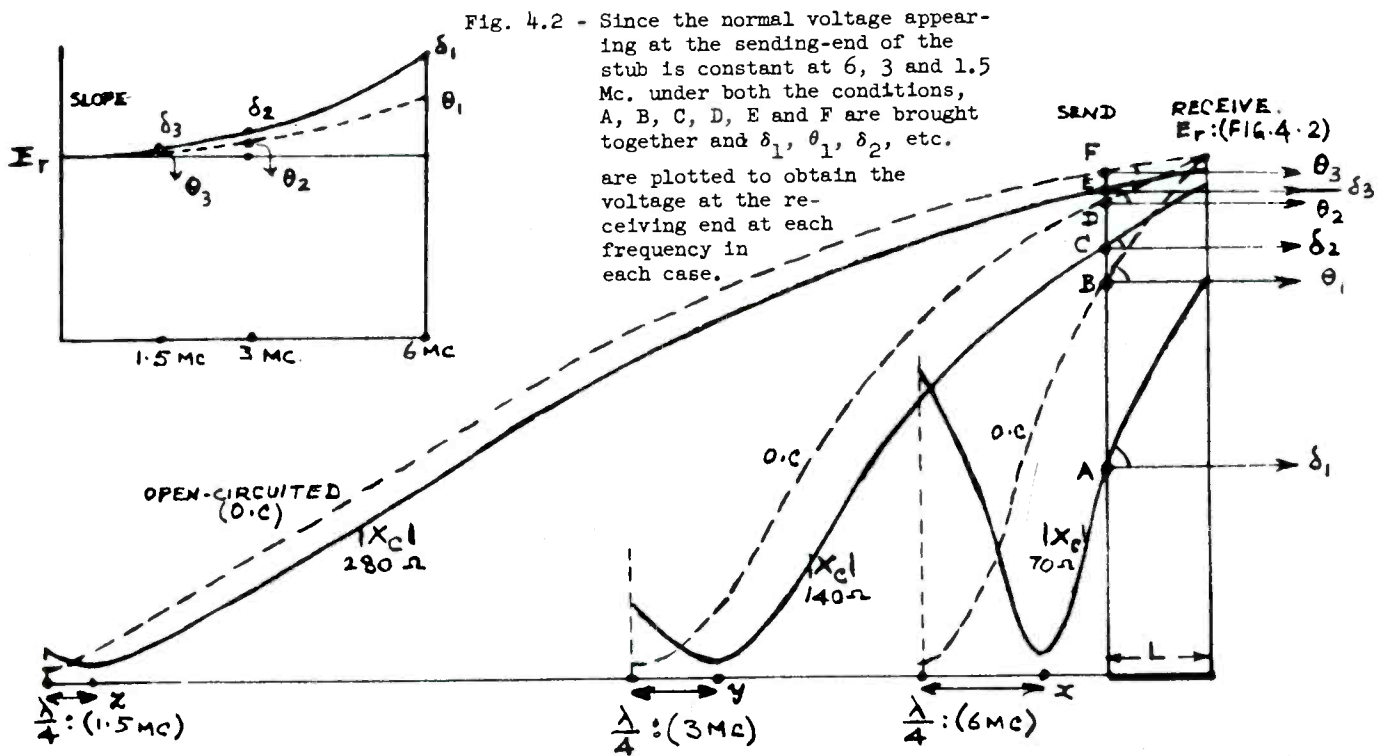


Fig. 4.2 - Since the normal voltage appearing at the sending-end of the stub is constant at 6, 3 and 1.5 Mc. under both the conditions, A, B, C, D, E and F are brought together and  $\delta_1$ ,  $\theta_1$ ,  $\delta_2$ , etc. are plotted to obtain the voltage at the receiving end at each frequency in each case.

Fig. 4.1 - The voltage distribution characteristics of the resonant coaxial-stub at 6, 3 and 1.5 Mc. Curves in dotted lines: Open-circuit at the receiving-end. Curves in full lines: Capacitive-reactance termination at the receiving-end.

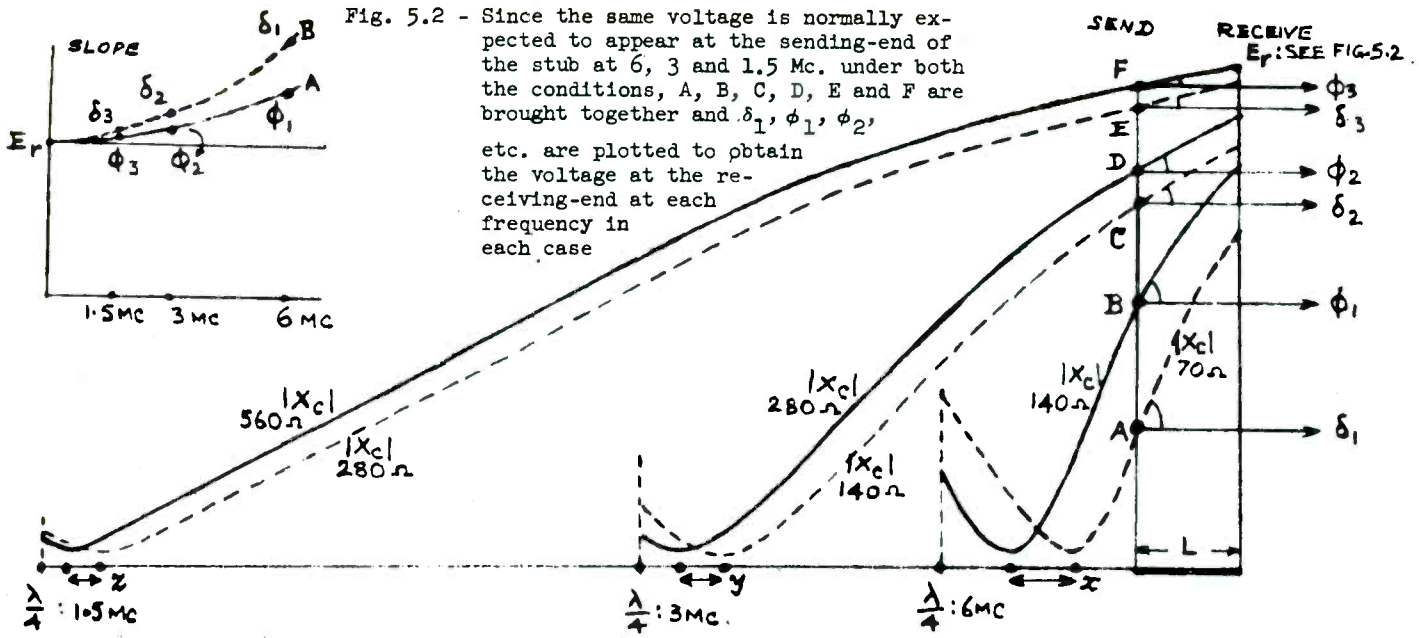


Fig. 5.2 - Since the same voltage is normally expected to appear at the sending-end of the stub at 6, 3 and 1.5 Mc. under both the conditions, A, B, C, D, E and F are brought together and  $\delta_1, \phi_1, \phi_2,$  etc. are plotted to obtain the voltage at the receiving-end at each frequency in each case

Fig. 5.1 - The voltage distribution characteristics of the coaxial-stub at 6, 3 and 1.5 Mc., depicting its performance as an automatic equalizer when it is terminated by a changing capacitive-reactance. Curves in dotted lines:  $X_c$  termination corresponding to 400  $\mu\mu\text{F}$ . Curves in full lines:  $X_c$  termination corresponding to 200  $\mu\mu\text{F}$ .

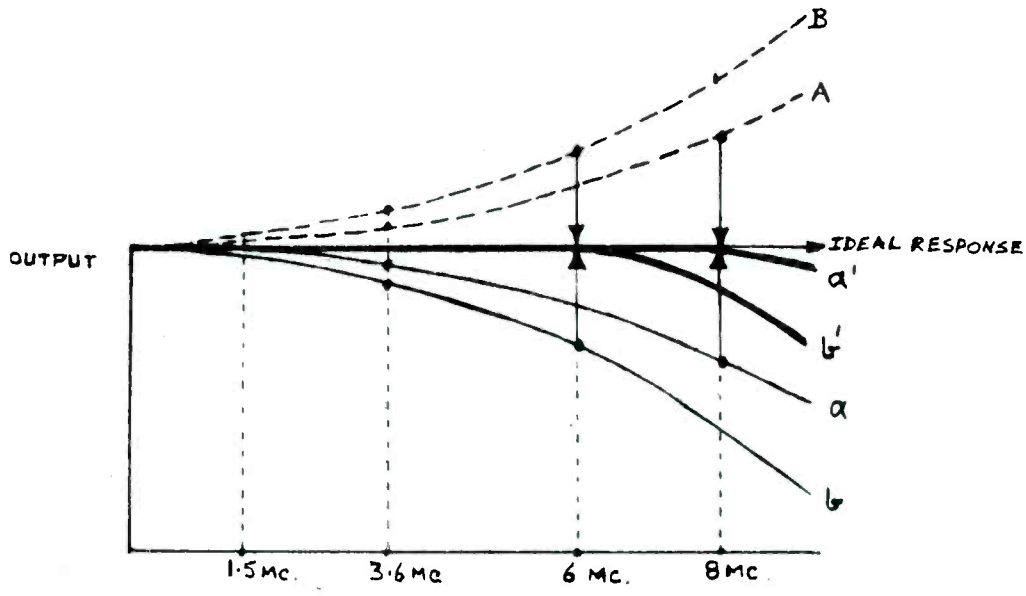


Fig. 6 - Curves a and a': Frequency response characteristics of the system with  $X_c$  termination corresponding to 200  $\mu\mu\text{F}$  across the receiving-end before and after equalization respectively.  
 Curves b and b': Same as above, with  $X_c$  termination corresponding to 400  $\mu\mu\text{F}$ .  
 Curves A and B: Voltage output versus frequency characteristics of the coaxial-stub (from Fig. 5.2) with  $X_c$  terminations corresponding to 200 and 400  $\mu\mu\text{F}$  respectively.

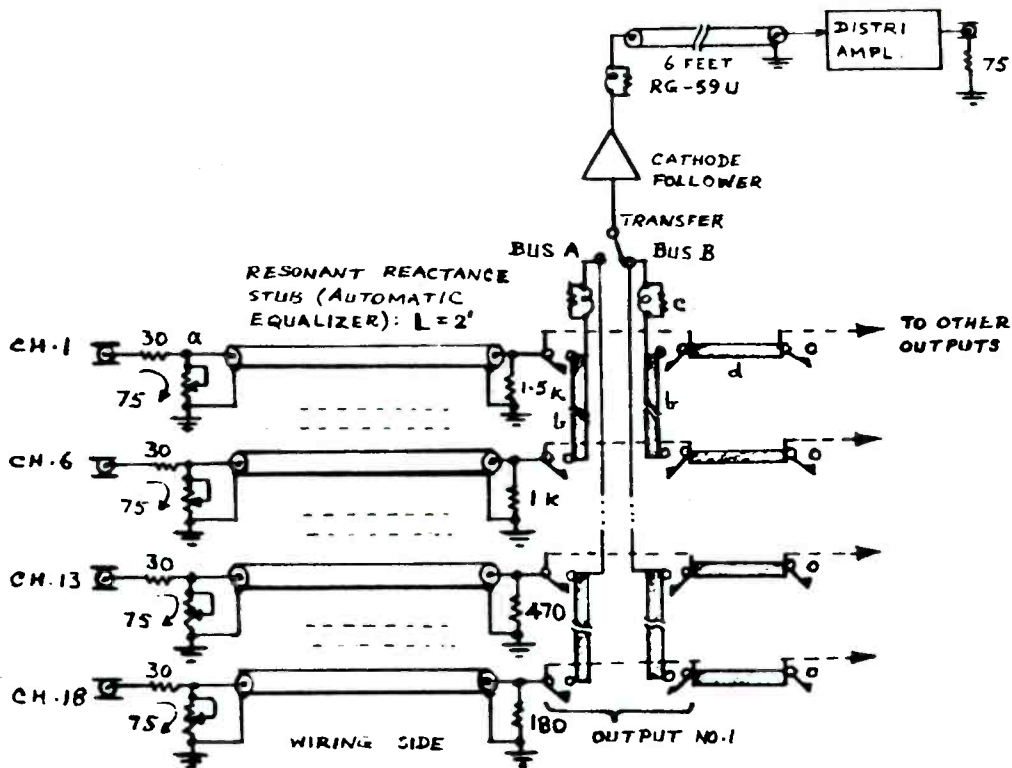


Fig. 7 - 18-channel, combined color and monochrome video switching system with provision of automatic equalization.

- a: 75-ohm channel input termination is split to lower inter-channel cross-talk at 3.58 Mc. to a negligible level, below - 40 db, under the worst switching conditions.
- d,b: Video input and output buses (copper strip, half-inch wide) are mounted in a slanting position. (Video output buses b are mounted on the opposite side.)
- c: Partial compensation for the connecting leads extending to the two lower six-channel groups. Resistors 1.5K, 1K, 470, 180, etc. present the variable-slope technique employed for each video channel in order to compensate the stub-effect of the longer video output buses. The path-length delay is thereby equalized at 3.58 Mc.

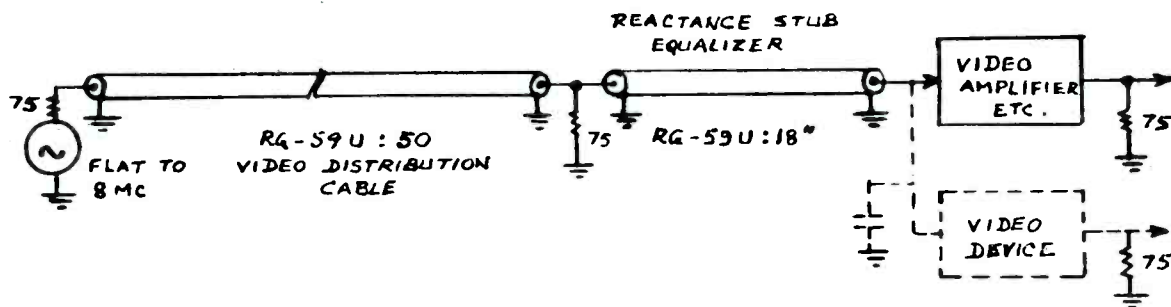


Fig. 8 - Coaxial-stub equalization for general video distribution cables (like RG-59U) inside the studio.

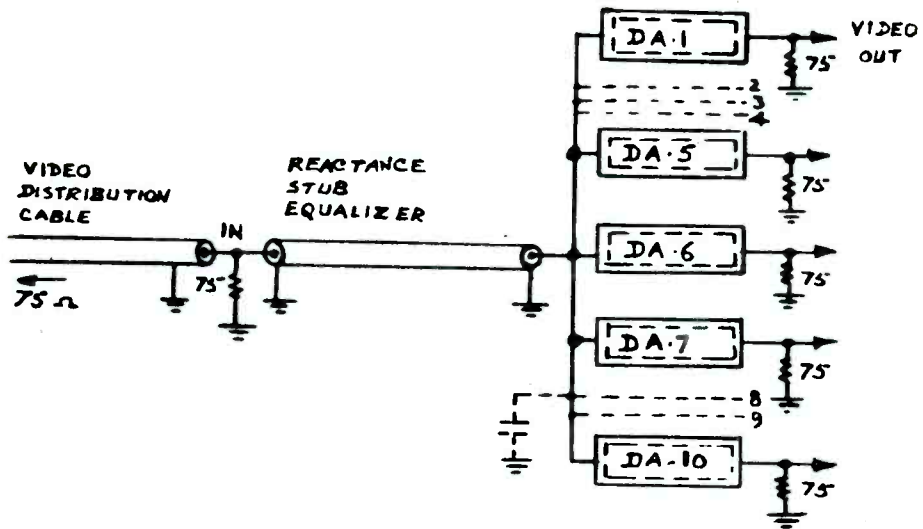


Fig. 9 - Improved video distribution system with resonant coaxial-stub equalizer. Each individual video output can be maintained at all times flat to 8 Mc. with DA modules 2, 3, 8, etc. plugged "IN" or "OUT" of circuit.

## TELEVISION ANTENNA SYSTEM MEASUREMENTS BASED ON PULSE TECHNIQUES

Donald W. Peterson

### I. Echo effects in a TV antenna system

The typical modern TV broadcasting antenna is mounted on a tower perhaps 1000 to 1500 feet high. The tower may be several hundred feet from the transmitter. This means that transmission lines for delivery of transmitter power to the antenna will be in the order of 1000 to 2000 feet long. Most lines in use are 3", 6", and 9" coaxial lines although waveguide is used in some systems. There is a trend toward lines both longer and larger than the 3" size used in early systems. Ordinarily, there are 3 or 4 elbows and a gas stop somewhere in the vicinity of the antenna and half a dozen or more elbows and a gas stop near the line input. The ground-level fittings are likely to be in two groups with a pair of elbows at the base of the long vertical run of line and several fittings near the line input.

After a new system has been installed it is necessary to establish that performance is normal. Excessive mismatch of the line termination (the antenna) or line faults will cause echo effects (ghosts or edge distortion), in the picture. There is also a possibility of line faults which do not produce visible echoes but which may sooner or later result in failures with the high transmitter power. Rather high line currents in the order of 25 amperes are not uncommon. Line faults can result from human error or mechanical failure during either manufacture or installation. When a system is not functioning normally it becomes necessary to locate and correct line or termination faults.

### II. VSWR specifications and trouble shooting

Specifications for transmission line, elbows, gas stops, and the line termination have customarily been in terms of voltage standing wave ratios (VSWR's). This is a perfectly satisfactory way of specifying these items as long as their performance can be measured individually. For example, the antenna VSWR can be measured at the antenna terminals before erection on the tower to learn if the line terminating impedance is normal. After the antenna, the line, 2 gas stops, and a dozen or so elbows are assembled,

the use of VSWR tests is anything but satisfactory for the over-all system. The reason will become clear upon consideration of a normal system.

Let us assume an antenna reflection coefficient of 4% (VSWR = 1.083), constant over the channel, and three elbows and a gas stop near the antenna each with a reflection coefficient of 1%. If there were no other discontinuities in the system, the reflection coefficient measured at the long line input could be constant or slowly varying with values between 0% and 8% depending upon the relative phase angles of the respective mismatching impedances.<sup>1</sup> The VSWR equivalent to 8% is 1.17. On the other hand, as many as seven more elbows and a gas stop near the line input would be more usual. Then the reflection coefficient measured at the line input could be anything from 0% to 16%. In the latter case, the VSWR could oscillate rapidly (from 1.0 to 1.38) with frequency over the channel while in the former case if there were any oscillations they would be much slower.

In the example cited the antenna echo voltage would be unchanged in going from the first situation with a maximum VSWR of 1.17 to the second situation with a maximum VSWR of 1.38. An echo voltage with enough time delay to produce a separate ghost image is much more conspicuous in a picture than the same echo voltage occurring at a brightness transition. Consequently, the widely disparate VSWR values of 1.17 and 1.38 produce essentially the same picture effect for the conditions given.

In any except the simplest situations it is hardly possible on the basis of VSWR (or reflection coefficient) data measured at the input of a complete system to learn accurately what the picture performance will be. Picture performance can be predicted only by deduction from VSWR's vs. frequency and then only in the simpler situations. If there is trouble in the system it is likewise difficult to impossible to locate the cause by VSWR measurements except in the simplest cases. It may also be noted that the trend toward longer and larger lines tends to increase the probable input VSWR without

---

1. Reflection coefficients may be simply added to obtain the maximum possible value when they are as small as the normal values in TV antenna systems.

necessarily degrading the picture significantly.

Another contributor to the difficulty of prediction of picture performance from VSWR data is the VSWR of the line itself. A normal, well-terminated long line always exhibits a rapidly varying input VSWR like that shown in Fig. 1. The line reflections may also add to the reflection from antenna and fittings to help produce sharp peaks in the over-all reflection coefficient at certain frequencies.

It is of considerable significance that a high reflection at a side band frequency produces a smaller echo voltage if low echo components from the vicinity of carrier frequency accompany the sideband echo. This means that having a low reflection coefficient near carrier is of greater importance than elsewhere. An unfortunate consequence of the use of VSWR proof of performance measurements and VSWR trouble shooting has been the neglect of this fact.

### III. Pulse echoes for locating faults

Pulse echo techniques have proven valuable for a variety of transmission line applications. Rather surprisingly they have found relatively little use in TV antenna systems. Both extremely short pulses and relatively long r-f pulses are effective in evaluating TV antenna system performance and locating faults.

Short pulses, which are substantially shorter than the shortest video pulse possible in a TV system, may be used to accurately locate line faults. A 0.01 microsecond "video" pulse with a spectrum out to 100 mc can be used to locate discontinuities so small that they produce only a 1% r-f echo on channel 13. Used with a scope having a rise time of 0.01 microsecond, faults can be located to within a few feet.

R-f pulses provide a means of measuring the echo voltages from the antenna and the aggregate of fittings near the antenna. In a normal system the antenna impedance produces the largest echo. To separate this from other possible accidental echoes in the system the shortest pulse which the system can pass should be used. Since the TV system is bandlimited to 4.25 mc and is a vestigial side band system, it will be necessary to pass the modulating pulse through the standard 4.25 mc filter and use a

demodulator with standardized receiver characteristics for measuring the antenna relative echo voltage. This will insure that side band echoes from the antenna, which may occur at frequencies outside the channel, will not appear as part of the total echo voltage. The relative echo voltage from the antenna is a measure of the picture performance to be expected with respect to the long line termination ghost.

Pulse measurements have been made on nine antenna systems,<sup>2</sup> some normal and some with trouble. The procedures used will be described and illustrative examples given. As an aid in the application of pulse techniques a number of deliberately introduced kinds of faults in a laboratory system were also used to show the special character of the echo voltages. These make it possible to learn the nature of the line faults from oscillograms of fully installed systems.

### IV. Short "video" pulse echo tests

Coaxial lines are commonly installed in lengths of 20 feet or a little less. It will therefore be convenient to be able to resolve faults spaced a minimum of about 20 feet. This requires a scope with a rise time of about 0.01 microsecond such as the Tektronix 545 with the 53/54L plug-in preamplifier. "Video" pulses as short as 0.001 microsecond are easily generated with a mercury wetted-contact relay and a pulse forming line.<sup>3</sup> The pulse repetition rate with such a device is line frequency. A commercial unit producing 0.001 to 0.1 microsecond pulses is the EPIC 200 square pulse generator, with a 60 p. p. s. repetition rate.

The pulse generator is connected directly to the line to be tested. See Fig. 2 for a block diagram. The scope terminals are bridged across the line. There should be a matched attenuator (about 10 db) between the generator and the scope so that the initial pulse and echo pulses "see" the same impedance at the scope terminals. The pad as "seen" by the echo pulse should have the same impedance as the characteristic impedance of the line under test.

2. These include WTAE, Pittsburgh; WJZ, WMAR, WBAL, Baltimore, WREC, Memphis; WOIA, San Antonio.

3. E. J. Martin, Jr., "Calibrated source of millimicrosecond pulse," Electronics, April 17, 1959.

The test pulse used is shown in the scope photo of Fig. 3. Photographs were made with a Polaroid Land 95A camera using type 44 film and 10 seconds exposure time. By advancing the scope gain by a factor of 100, the echoes of Fig. 4(a) are seen from a normal 3" RCA universal line. This line has been designed with "transparent" teflon insulators and is of a quality suitable for both VHF and UHF TV. Another high quality line, a Styroflex 51.5 ohm line yielded the pulse photo of Fig. 4(b).

With the equipment used, echoes from discontinuities spaced 20' may be resolved. The resolution can be increased by a factor of ten by use of a faster scope. However, it is believed that 20 foot resolution is adequate for practical purposes. Accuracy of the scope sweep calibration is 2%. This accuracy may be improved upon by use of a periodic marker of accurately determined frequency. This refinement likewise seems hardly necessary because of the ease of obtaining a reference echo at a known location by simply opening or shorting the long line near a fault. The resolution capability is illustrated in the photos of Fig. 5 where the echoes from 2 or 15 discontinuities, deliberately spaced 20 feet along a 3" coaxial line, are seen.

The character of the echo voltage reveals the nature of the cause. Echoes from a short and an open circuit are shown in Fig. 6. A shunt resistor, a transition to a line of lower characteristic impedance, or a branch line produces an echo like that of the short circuit but of lesser magnitude. A series resistance or a transition to a line of higher impedance produces an echo like that of an open circuit but of lesser magnitude. The echo from a shunt lumped capacitance is also shown in Fig. 6.

The echo from an inner coupling with poor and intermittent contact is shown in Fig. 7. Also shown is the echo from an accidental shunt capacitance. Both of these effects were seen only by advancing the scope gain by a factor of about 100. A common line fault is the failure to properly join the inner conductor coupling. The echo from a mismatched coupling is shown in Fig. 7.

Something about the antenna itself may also be learned from pulse echoes.

Each antenna type yields a characteristic pulse echo record. The return from an RCA 6 bay super-turnstile antenna is shown in Fig. 8(a). The first echo comes from the junction of the main 50 ohm coaxial line and the twelve  $77\frac{1}{2}$  ohm feeder lines of the antenna, a junction where the impedance "seen" by the initial pulse is  $77\frac{1}{2}/12$  or 6.5 ohms. The second echo is a return from the shorting bars of the radiators and subsequent echoes are "re-bounds" between these two impedance changes. A 12 bay super-turnstile produced the echo of Fig. 8(b). The echo returned from an RCA traveling wave antenna is shown in Fig. 8(c). The first echo is from the shorting bar at the antenna base. Subsequent echoes are from "re-bounds" between the shorting bar at the upper end of the antenna and the base. By advancing the scope gain, echoes from normal line discontinuities, which are distributed along the antenna, may be seen.

It should be remembered in studying short pulse photos that an r-f transformer is usually too short to enable resolving the echoes from the changes in impedance at both transformer terminals. Therefore, a transformer echo does not fully reveal the character of the transformer. However, the change of impedance of the two lines into which the transformer has been inserted will be in evidence.

Short pulse echoes have been successfully used in installed systems for locating opens, shorts, burned couplings which were still operating satisfactorily, noisy couplings, matching slugs, and changes of characteristic impedance. As a trouble shooting tool, the method is invaluable. The pulse record of a line also serves very effectively to establish the normalcy of the line. While short pulse tests do not directly show picture performance for the r-f channel of interest, they have value in establishing normalcy based on tests of lines which are known to be normal. By preserving pulse photos of an installation it becomes possible, if trouble later develops, to trouble shoot with speed, precision, and assurance.

#### V. R-f pulse echo tests

The same Tektronix 545 scope may be used for r-f tests. However, the usual TV station scope will also suffice. A pulse generator such as the Hewlett Packard 212A with continuously variable pulse width is desirable. The r-f source may be a General Radio 1021 signal generator or the equivalent. The r-f is pulse modulated with a General Radio 1000 P1 crystal diode modulator. The VHF spectrum requires the General Radio P3 plug-in oscillator, the UHF requires the GR P2 oscillator.

The r-f pulse source is connected through an r-f amplifier, such as RCA Mastertenna HG, to the line to be tested. See Fig. 2 for a block diagram. A demodulator, such as RCA BW4B with a standardized receiver characteristic, is used for detection. This makes it possible to make pulse tests either with or without a VSB filter. The demodulator input is bridged across the long line input.

For tests of the line termination, that is, the antenna impedance, it is necessary that the pulse spectrum used be the same as the transmitter and VSBF normally deliver because antenna match is required only over that spectrum. Proper pulse spectrum limitation is accomplished by high frequency cut-off with an RCA M127132 filter, the same filter ordinarily used with the TV system and by using the RCA BW4B demodulator or the equivalent.

There should be an attenuator pad (about 10 db) at the r-f amplifier output and the demodulator input impedance should be altered so that the echo pulse "sees" the line characteristic impedance  $Z_0$  at the demodulator terminals. Suitable attenuators are made by Microlab and others. There should also be a line stretcher between the demodulator and the line under test for a reason to be explained.

The two pulse widths which have been found useful enable tests of both the line and the termination. The shortest pulse that the TV system will handle is useful for measuring the reflection from the long line termination. Tests have been performed with a "black" pulse using about 80% modulation.

Since there will ordinarily be less than 100% modulation with either the test set-up or the TV transmitter, there will be continuous r-f coming from the signal source, either from the "black" pulse or the "white" background. When an echo voltage returns from the line termination this will add to the "white level" r-f coming from the generator at the time the echo pulse arrives. The relative r-f phase will depend upon the line lengths between demodulator and long line termination and between demodulator and generator. The line stretcher may be used to adjust the relative phase to produce demodulated echo voltage of the same or opposite polarity as the initial pulse. That is, either a positive or a negative ghost is produced. An echo having the same polarity as the initial pulse is

usually chosen for the measurement.

A calibrating means is required for determining the magnitude of the echo pulse. It is the ratio of the maximum echo pulse to the initial pulse, or the relative reflection voltage that is desired. This will be the maximum relative echo voltage that can be produced by the system. Calibration at the 5% relative echo voltage level, for example, is accomplished by terminating the flexible coaxial line, used for connecting to the line under test, with a matching resistor. Then the pulse magnitude is adjusted to scope full scale, after which 26 db (20:1) matched attenuator is inserted between the r-f amplifier and the demodulator. This gives the 5% calibrating level on the scope. Then the scope gain is advanced by a known factor to cause the 5% level to occur with increased scope deflection.

It should be noted that a line termination measurement with an r-f pulse includes effects of elbows and seals near the antenna. This is well since it is the combined effect which determines the magnitude and character of the ghost produced in the radiated picture.

Some antennas, such as the RCA super-turnstile, are fed with two lines of equal length. A normal antenna presents identical terminating impedances to the two lines since the individual lines respectively feed the identical North-South and East-West halves of the antenna. At the bridge diplexer which feeds the lines an extra quarter wave phasing line is inserted in one of the lines, say the EW line as in Fig. 9. The antenna impedance should be measured at the long line inputs at the diplexer terminals. By adjusting the line stretcher for an echo of the same polarity as the initial pulse on say, line A, the opposite polarity echo pulse should be seen on line B if the antenna is normal. Echo pulses from a slightly unbalanced antenna, measured from the long line inputs at the diplexer are shown in Fig. 10.

A second test with r-f pulses requires a pulse longer than the round-trip propagation time of the long line. The purpose here is to test the long line itself. This test is more critical than may be made with the use of a short r-f pulse since the line may have equally spaced echoes which add because the echo voltages happen to all be in phase. This test supplements the short r-f pulse test and can be used to resolve doubts, if any exist after pulse tests, about the desirability of looking for line troubles. Again a line stretcher will be used for phase control. A normal line oscillogram is shown in Fig. 11. A line with multiple, evenly spaced discontinuities resulted in the oscillograms of Fig. 12.

The long r-f pulse test serves for evaluation of abnormal echoes which may be observed with short, "video" pulses. If an echo pulse observed with a "video" pulse is only a little larger than

the normal background clutter of echoes there may be a question of the advisability of undertaking to locate the cause. The "video" pulse measurement is sensitive enough to show many inconsequential echoes. On the other hand the causes of some echoes observed with "video" pulses, which are not apparent with r-f pulses, should be located because they may result in eventual trouble. An example would be a noisy coupling which appears as an intermittent echo with the "video" pulse test.

A photograph of test apparatus for both short "video" pulse and r-f pulse measurements is shown in Fig. 13.

#### VI. Over-All pulse test of a TV system

Sometimes there is doubt about the source of a small ghost in the picture as received in the field. There will commonly be propagation multipath ghosts in the picture which tend to obscure radiated ghosts or make uncertain their magnitude and character. A test through the entire system with pulse photos at appropriate places can quickly and with assurance establish what is wrong and where. A suitable pulse source would be either an electronic pulse generator capable of generating a vertical picture line or a slide camera with low noise.

The slide shown in Fig. 14 has been used for this purpose. A narrow white line on a black background and a narrow black line on a white background provide the test pulses. Using a line selector scope, a single line of the video waveform can be photographed at the studio, at the transmitter on the video line or microwave link output, at the picture transmitter output directional coupler, or individual lines feeding the two halves of a turnstile, and in the field in directions chosen to be on the maxima of the respective two halves of a turnstile antenna, for example.

Pulse photos on the two lines of a super-turnstile using such a signal source are shown in Fig. 15. These were also observed in the field where it was found that multipath signals tended to obscure the small radiated ghost.

#### VII/ The correspondence of monitor and field pictures with respect to ghost effects.

There seems to be a certain amount of confusion about the meaning of test

pulses observed on station picture and waveform monitors. There are in common use (1) broad band diodes for monitoring and (2) demodulators having a standardized receiver characteristic and using signal from directional couplers. The antenna systems use either a bridge diplexer or a filter for feeding both picture and sound transmitters into a common antenna.

Consider first an antenna system using a bridge diplexer such as the RCA super-turnstile. The NS and EW halves of a turnstile antenna normally present identical terminations to the long lines. The picture voltage enters the lines at points A and B of Fig. 9 out of phase. The echoes from the antenna halves return in phase because of the round trip traversal through the quarter wave section in only one line. Therefore, the echo voltage enters the sound line, is fully reflected by the sound transmitter and returns to points A and B in phase in the two lines. Since the initial voltages entering the lines at A and B were out of phase, the demodulated voltages in the two lines will have opposite polarities as observed with directional couplers at A and B oriented to "see" the wave traveling toward the antenna.

If the echo voltage returning to points A and B come from terminations which are not identical, the phases may not be alike, in which case some of the echo voltage will return to the picture transmitter to be at least partially reflected and to return to the antenna.

This system should be monitored at points A and B with signal coming from a directional coupler. Observation with a directional coupler at the output of the transmitter or at the diplexer input shows only part of the echo voltage on its way to the antenna if it shows anything. Monitoring on the picture input line of the diplexer or at the transmitter output with a diode is even worse because the relative amplitude of the echo voltage depends upon location along the line. Since all locations along the picture transmission line give results completely false with respect to radiated effects this is not the place to monitor ghosts from antenna mismatch with either diode or directional coupler.

By monitoring on the individual long lines with directional couplers at points A and B the true<sup>4</sup> radiated signal may be observed. Monitor point A shows the echo radiated by the EW antenna and B the echo radiated by the NS antenna.

If the system is balanced, that is, if demodulated echo voltages observed at A and B are equal and opposite, it may be possible to

4. Strictly, speaking, the true radiated signal can only be observed by monitoring the radiated field. In a normal, well engineered system, the monitoring locations designated give a very close approximation to the radiated signal.

minimize the radiated echo voltage by adjusting the length of the sound line. This has been done successfully although it is a limited remedy which depends upon equality of the impedances terminating the long lines. Thermal expansion of the line may make the radiated echo voltage unstable, particularly for ultra high frequencies.

Consider now a system with which the sound transmitter and picture transmitter outputs are combined with a filter to feed a single line. The echo voltage returns to the picture transmitter and is at least partially reflected. The polarity of the echo depends on the lengths of the line between the picture transmitter and the long line termination. Again, adjusting a line length, this time the long line or the line from picture transmitter to filter may minimize the echo voltage.

With such a system the picture observed with a directional coupler at the picture transmitter output shows long line echo voltages which will be seen on receivers in the field. However, the picture observed with a diode across the line may either exaggerate or reduce the echo voltage relative to the initial voltage depending on location of the diode.

#### VIII. Conclusion

Both short "video" pulses and r-f pulses have been shown to have great value for establishing the normalcy of new systems, for preventive maintenance, for observation of gradual deterioration, and for fault location. In the writer's judgment this kind of test should become the primary means of testing systems in the field. Other methods such as VSWR and resistance measurements should become subordinate aids. A complete pulse photo record for a new system will be well worth keeping on file in case trouble should develop.

#### Acknowledgement

The laboratory work and field tests were done in cooperation with E. N. Luddy and H. E. Gihring of the RCA Broadcast and Television Equipment Division, Camden, N. J.

#### References

E. D. Sunde, "Theoretical fundamentals of pulse transmission", Parts I and II, Bell System Technical Journal, May and July 1954.

A. C. Beck, "Waveguide investigation with millimicrosecond pulses", Bell System Technical Journal, Jan. 1956.

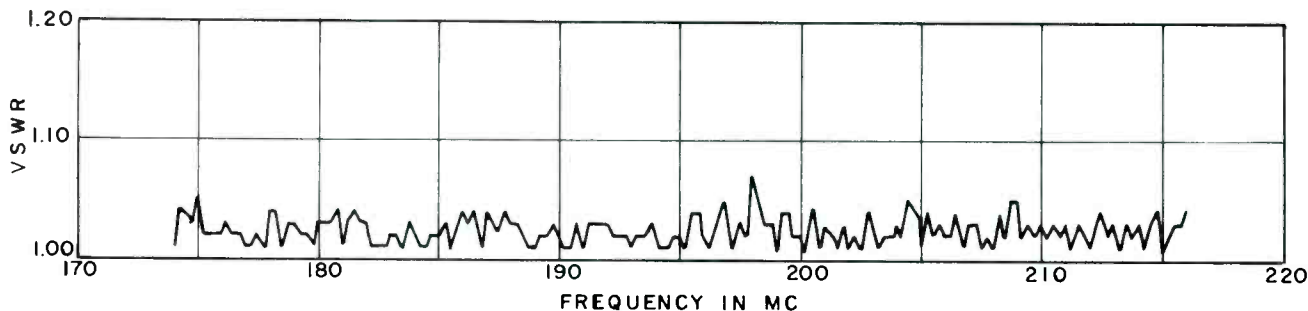
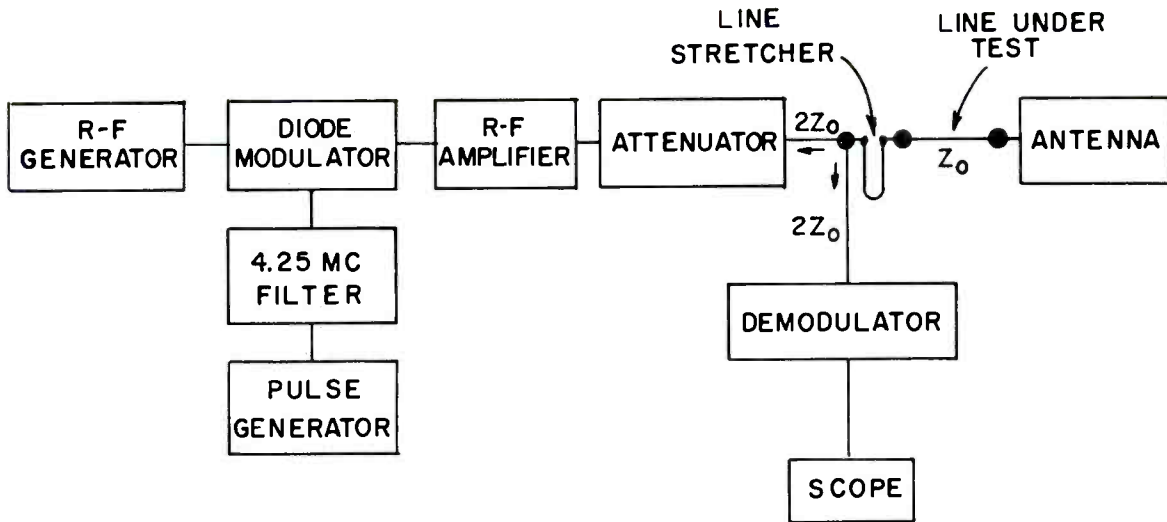
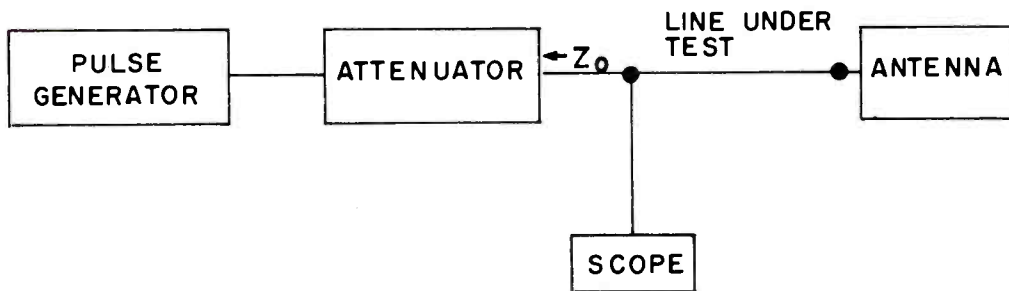


Fig. 1 - Input VSWR of 800' of high quality transmission line terminated in its characteristic impedance.

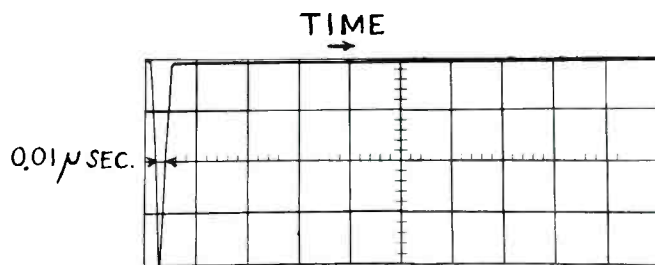


R-F PULSE TEST



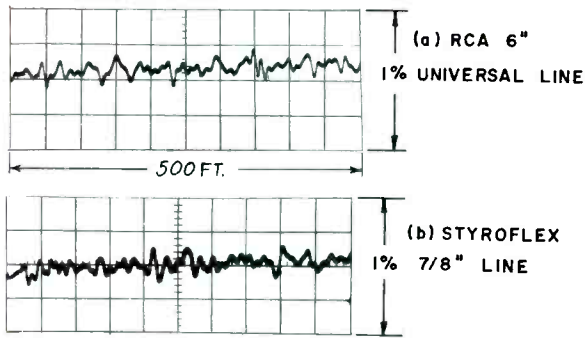
D-C PULSE TEST

Fig. 2



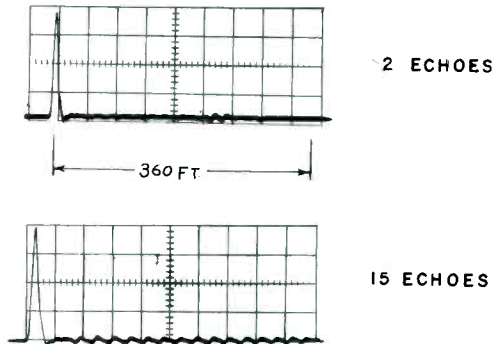
TEST PULSE

Fig. 3



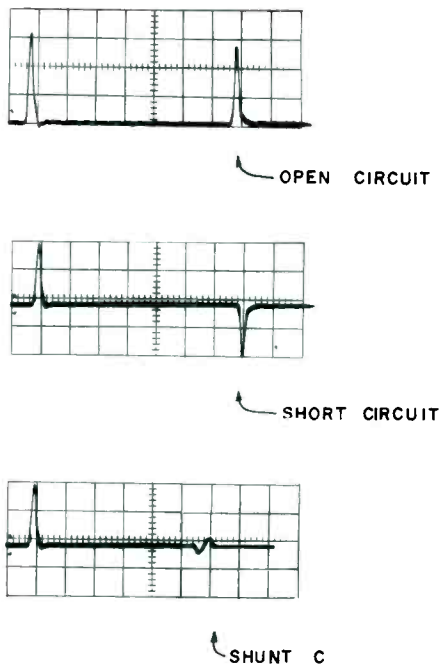
DC PULSE ECHOES FROM NORMAL HIGH QUALITY LINES

Fig. 4



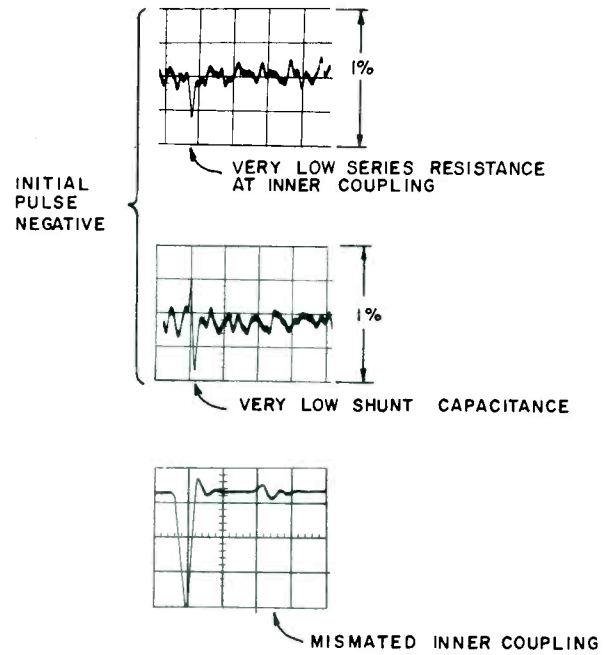
DC PULSE ECHOES FROM SHUNT C SPACED 20 FEET

Fig. 5



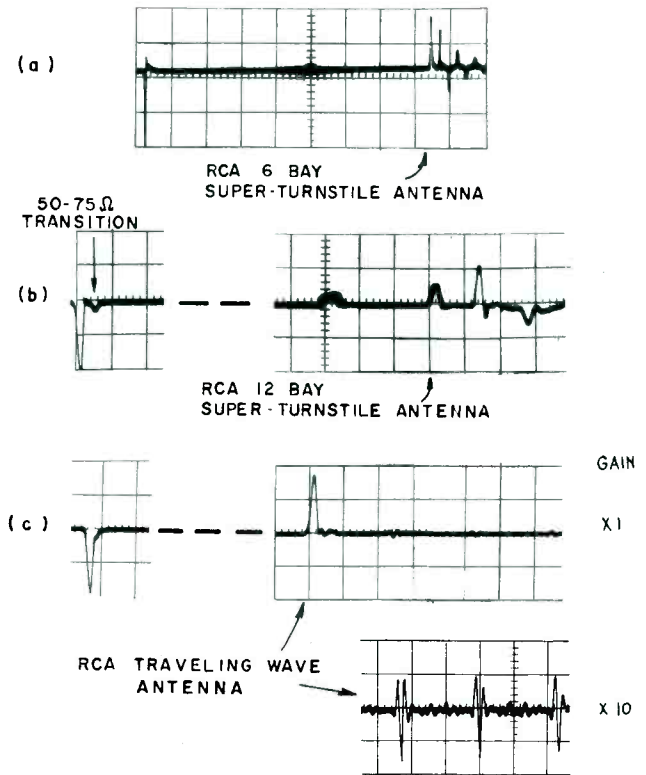
DC PULSE ECHOES

Fig. 6



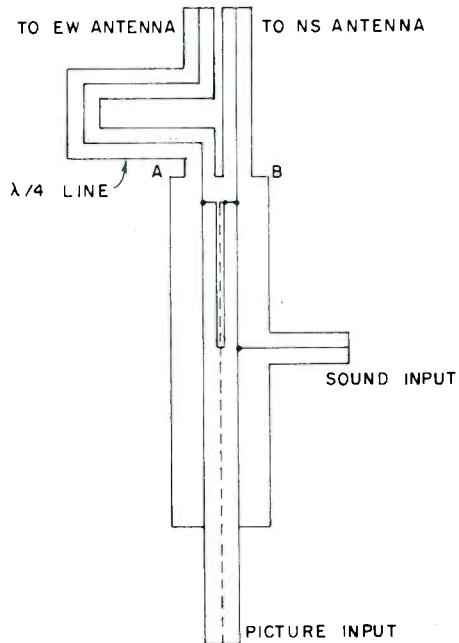
LINE TROUBLES LOCATED WITH DC PULSES

Fig. 7



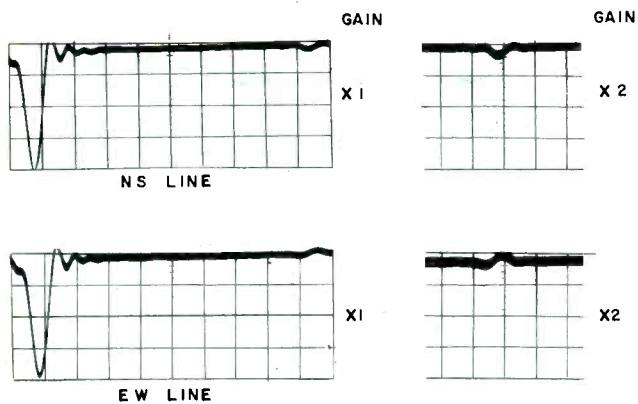
PULSE ECHOES FROM SEVERAL ANTENNAS

Fig. 8



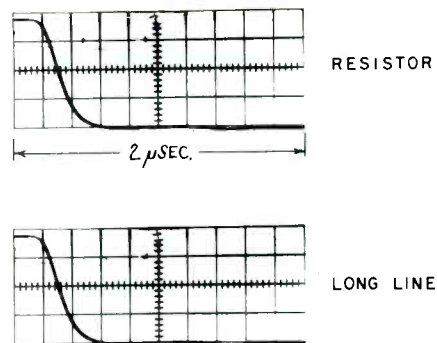
BRIDGE DIPLEXER

Fig. 9



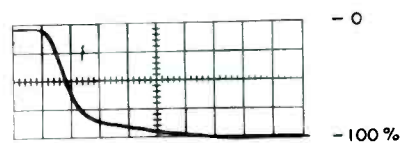
R-F PULSE APPLIED TO MEASUREMENT OF A LONG LINE TERMINATION

Fig. 10

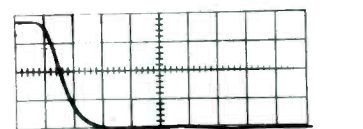


RF PULSE APPLIED TO A NORMAL 3" LINE

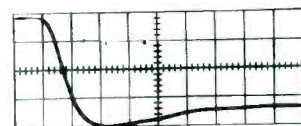
Fig. 11



IN PHASE END OF LINE



INTERMEDIATE PHASE END OF LINE



OUT OF PHASE END OF LINE

R-F PULSE APPLIED TO 3" LINE WITH PERIODIC SHUNT C

Fig. 12

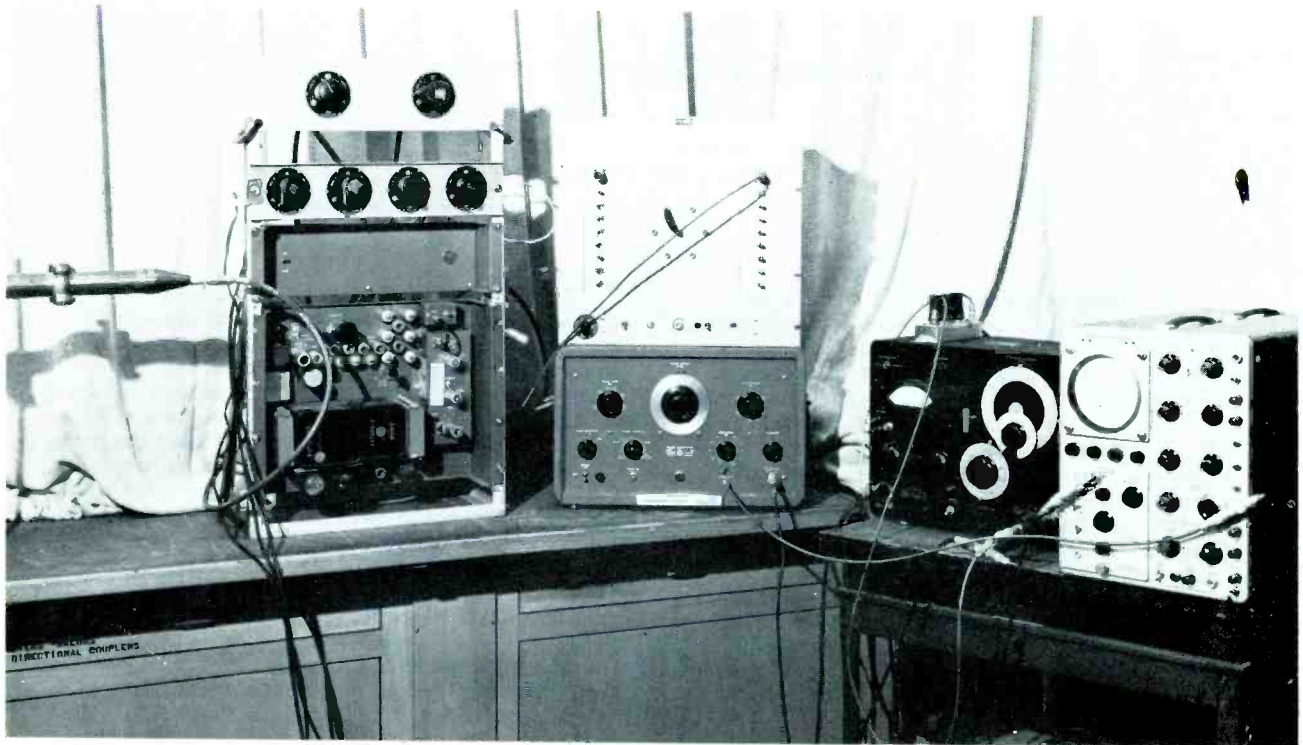


Fig. 13



SLIDE FOR OVER-ALL SYSTEM TEST

Fig. 14

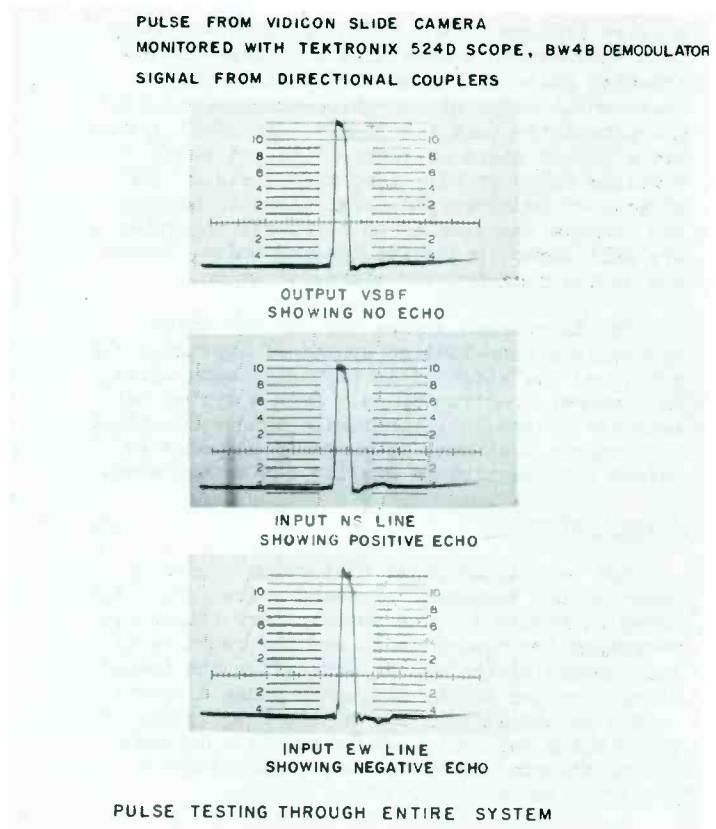


Fig. 15

## NEW EQUIPMENT FOR MEASURING ENVELOPE DELAY

Edward Noel Luddy  
Radio Corporation of America  
Camden, New Jersey

### Summary

The envelope delay characteristic is an extremely important factor in television systems. The effect of improper envelope delay is quite pronounced in color television, but a properly corrected system is also necessary for monochrome transmission if the optimum in picture quality is to be obtained. A new measuring technique has been developed which provides a low frequency reference to properly relate the envelope delay of the high and low frequency components of the video signal. The RCA BW-8A Envelope Delay Measuring Set utilizes this new technique, and is designed for television station use. This paper highlights the importance of the envelope delay characteristic and describes the new measurement technique.

### Envelope Delay

The phase-versus-frequency characteristic of television systems is usually referred to in terms of time delay or envelope delay. Time delay is equal to the phase shift divided by the angular frequency ( $\phi / 2\pi f$ ). Envelope delay is a somewhat more sensitive term used for expressing phase shift, and is equal to the incremental slope of the phase-versus-frequency characteristic ( $\Delta\phi / 2\pi\Delta f$ ). An ideal system has a linear phase characteristic and equal envelope delay at all video frequencies. The effects of improper phase relationship between the various frequencies in a television system are well known, producing leading white, trailing smear, ringing, and misregistration.

The television system used in the United States is a band-limited system of approximately 4 mc, and one sideband is partially attenuated to conserve spectrum space. Such a system has many advantages, but inherently introduces phase distortions that must be properly compensated before optimum picture quality can be achieved.

### Phase Distortion

The results of phase distortion caused by band-limited vestigial sideband transmission are shown in Figure 1. The anticipatory transients preceding the transitions, and the rounding of the corners of the square wave after the transitions, are due to low frequency phase distortion caused by the attenuation of the lower sideband. The ringing following the transitions is caused by the attenuation of the upper sideband and resulting phase distortion.

These defects resulting from delay distortions cannot be completely eliminated but can be reduced in magnitude. Figure 2 shows the square wave response of a system that has been corrected by means of phase correction networks in the video input circuit of the transmitter. The anticipatory transients preceding the transitions have been eliminated and the corners following the transitions have been made square. These improvements were made by correcting the low frequency phase characteristic. The ringing has been distributed before and after the transition, and reduced in magnitude by means of high frequency phase correction.

The FCC specifies the envelope delay characteristic required in the transmission of color television signals as shown in Figure 3. The relative envelope delay throughout the video region is referred to the average delay between 50 and 200 kilocycles and is required to be constant except in the region above 3 mc which is pre-distorted to compensate for the phase characteristic of the sound notch in a typical television receiver. The tolerances are shown by the dotted lines. The transmitter is required to correct only for its own phase distortion in the low frequency region and each receiver is to correct for any phase distortion it may introduce at the low frequencies.

### BW-8A Measuring Set

There is a need for field test equipment to measure the envelope delay characteristic of television transmitter systems in accordance with FCC specifications. Quantitative measurements have been rather difficult to make in the field, and many stations have made only approximate checks by means of square wave responses. The BW-8A Envelope Delay Measuring Set, shown in Figure 4, was designed to fill this need. It is a small unit, easy to use, and provides a low frequency phase reference. The BW-8A measures the relative envelope delay in the region from 1.3 mc to 4.3 mc as referred to the average delay between 0 and 189 kc. The unit is designed for standard 19" rack mounting, and occupies 10½" of rack space.

The BW-8A Envelope Delay Measuring Set consists of a generator section that feeds the system to be measured, and a receiver section which evaluates the envelope delay of the signals after they have passed through the system under

test. A block diagram of the unit is shown in Figure 5. A fixed modulating frequency of 189 kc can be obtained from an internal crystal oscillator or can be derived as the twelfth harmonic of the horizontal sync frequency supplied from an external source. Switch S1 selects the source of the modulating frequency and adds sync and blanking if desired.

The fixed 189 kc modulating signal is fed to a mixer amplifier together with a carrier frequency that is variable in the range of 1.3 mc to 4.3 mc. This carrier is modulated to a depth of about 50% by a portion of the output of the fixed 189 kc oscillator. The original 189 kc frequency and the modulated carrier frequency are recovered at the output of the mixer. Sync and blanking are added if desired, and the signal is amplified.

The output of the generator portion of the BW-8A can be fed directly to the receiver portion of the unit for calibration purposes. The output of the generator is then switched to the input of the transmitter system under test and the demodulated output of the transmitter is fed into the input of the receiver section.

The receiver section is composed of two chains. The first amplifier is tuned to the modulated carrier frequency. The signal is then detected and the 189 kc modulating component recovered. The demodulated signal is amplified and fed to a phase detector. The other amplifier chain is tuned to the 189 kc signal that has passed directly through the system. This signal is also amplified and fed into the phase detector. The phase shifter consists of an RLC network and may be switched into either amplifier chain to permit compensation of either positive or negative time delay. The phase shifter is calibrated directly in microseconds and reads the relative envelope delay between the carrier frequency and the reference average envelope delay between 0 and 189 kc. Envelope delays up to 0.68 microseconds may be measured with an accuracy of  $\pm (3\% \pm .01)$  microseconds.

#### Typical Test Set-up

A typical test set-up using the BW-8A Envelope Delay Measuring Set is shown in Figure 6. The output of the generator section is fed to the video input of the transmitter ahead of the phase equalizers and low pass filter. It may be fed into the input of the stabilizing amplifier if sync and blanking are added. The output of the transmitter must be demodulated to recover the video component. A standard vestigial demodulator such as the RCA BW-4B can be used for this purpose, or a diode may be employed. The output of the vestigial demodulator or diode is fed to the receiver section of the BW-8A.

#### Envelope Delay Characteristics

The envelope delay characteristic is specified by the FCC in terms of a perfect vestigial demodulator. Standard demodulators, such as the RCA BW-4B, approach the ideal receiver characteristics within very close limits. A standard vestigial demodulator should be used to monitor television signals at the output of the sideband filter as it will provide the best indication of picture quality as viewed on good home receivers.

When fed with a vestigial sideband signal, the diode demodulator not only provides a non-uniform video amplitude response, but also a distorted phase characteristic as shown in Figure 7. Although vestigial sideband signals cannot be satisfactorily monitored from a diode demodulator, it was deemed desirable to be able to use this type of demodulator to measure the envelope delay characteristic of the transmitter system. By utilizing the diode as a check against the vestigial demodulator, the error due to a poorly aligned or poorly compensated vestigial demodulator can be isolated.

The calculated envelope delay characteristics of a television transmitter and filterplexer combination that is not phase compensated is shown in Figure 7. Calculated curves for both a diode demodulator and an ideal vestigial demodulator are shown. It can be seen that in the low frequency region where a double sideband signal is available the two demodulators provide essentially the same overall envelope delay. In the region where the lower sideband is being attenuated the two curves differ quite widely. After the lower sideband has been attenuated the two envelope delay curves become identical. This indicates that a diode demodulator can be used to determine the envelope delay characteristic of video frequencies above approximately 1.5 mc as compared with a reference in the range below 200 kc. This is the important region to be investigated as the envelope delay in the range from approximately 200 kc to 1.5 mc is controlled only by minimum phase shift networks as far as the transmitter is concerned. Variations in the phase characteristic of the transmitter upper sideband in this region are related to the amplitude response which is generally quite flat at these relatively low modulating frequencies. The overall video phase response in this area is largely dependent on the degree to which the demodulator that is used accepts or rejects the lower sideband.

The envelope delay characteristic of a visual modulator as measured by the BW-8A is shown in Figure 8. The modulator alone contributes relatively little delay except at the very high frequency end where the frequency response is being attenuated. The overall transmitter envelope delay characteristic utilizing a diode demodulator

is also shown in Figure 8. Only minor variations in the basic transmitter envelope delay response are experienced before sideband shaping is applied.

The envelope delay of a television transmitter and vestigial sideband filter is shown in Figure 9. No phase correction was employed in the transmitter input, and the need for about 0.15 microsecond low frequency equalization is apparent. The measurements taken with the diode demodulator and vestigial demodulator agree quite closely in the range from 1.3 mc to 4.3 mc. Either type of demodulator may be used with the BW-8A Envelope Delay Measuring Set.

The final overall envelope delay characteristic is usually taken with all phase correction networks in the circuit including properly adjusted low frequency and receiver equalizers. An overall envelope delay curve of an RCA TT-11AH Transmitter is shown in Figure 10. The curve shows the relative delay at various video modulating frequencies as compared with the average

envelope delay between 0 and 189 kc. The FCC tolerances are shown by the dotted curves.

#### Conclusions

It is vital that television transmitting systems be properly corrected for envelope delay deficiencies in order to broadcast high quality pictures. It is hoped that the BW-8A Envelope Delay Measuring Set will make it easier to test and align television transmitting systems to improve the fidelity of transmission.

#### Acknowledgments

The author wishes to express his gratitude to C. D. Kentner, Manager of Broadcast Transmitter Development and Measuring Equipment Design, and J. C. Chianbrando of Broadcast Transmitter Engineering for their contributions to this paper and the design and test of the BW-8A Envelope Delay Measuring Set.

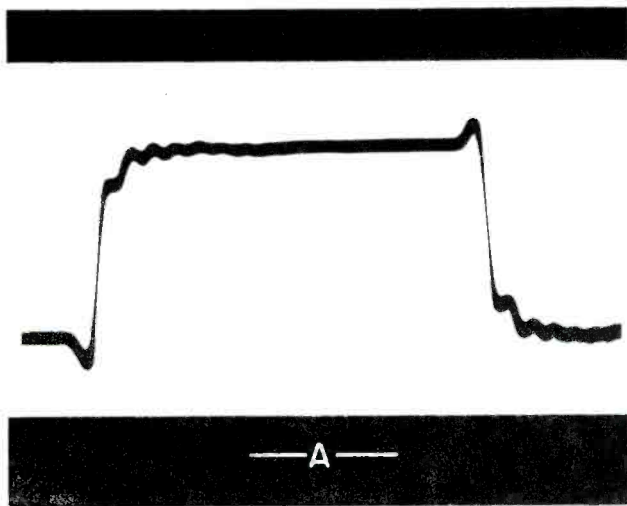


Fig. 1 - Typical uncorrected TV system response of 100 kc square wave.

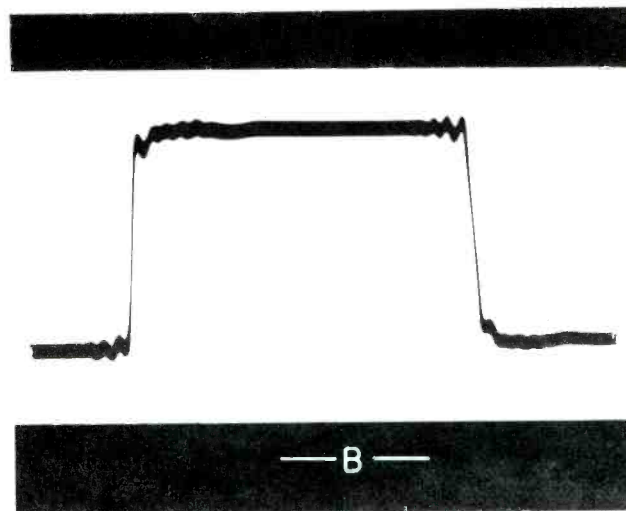


Fig. 2 - Typical phase corrected TV system response of 100 kc square wave.

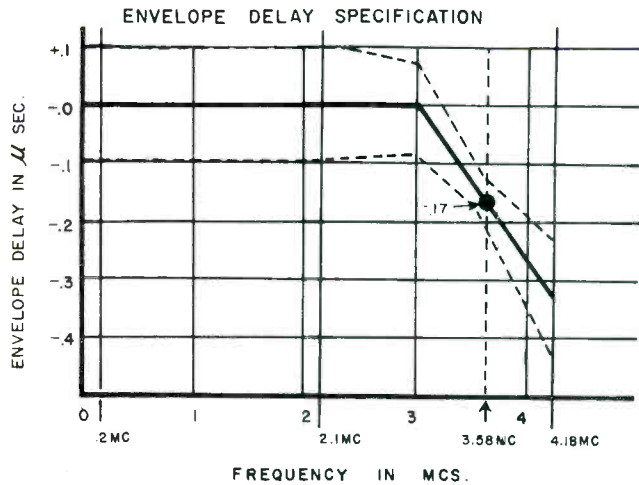


Fig. 3 - FCC transmitter envelope delay curve for color TV transmission.



Fig. 4 - RCA Type BW-8A envelope delay measuring set.

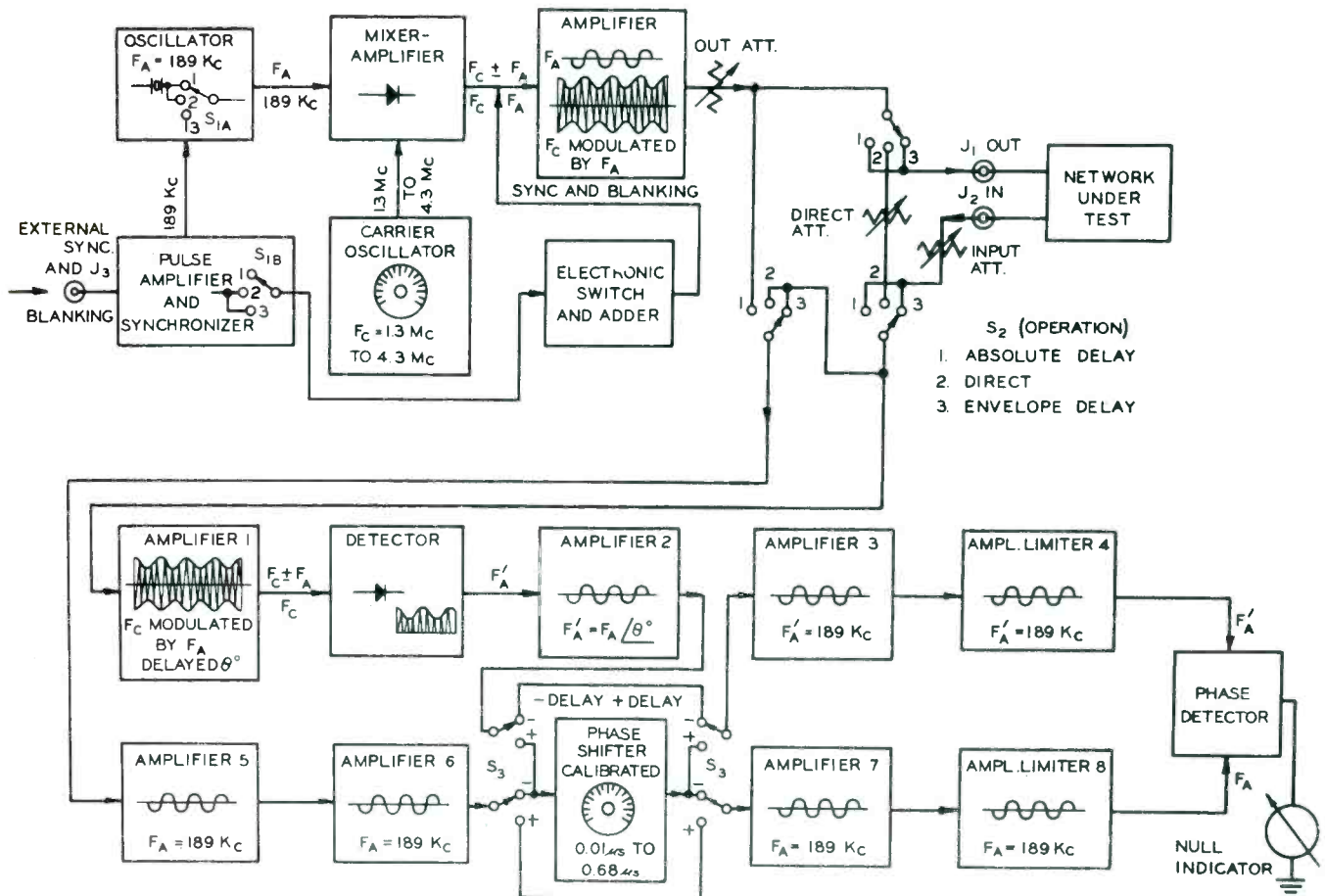


Fig. 5 - Block diagram of RCA BW-8A envelope delay measuring set.

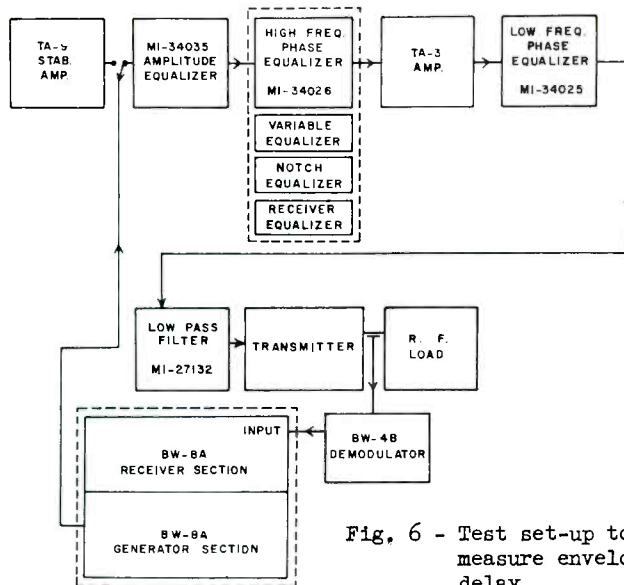


Fig. 6 - Test set-up to measure envelope delay.

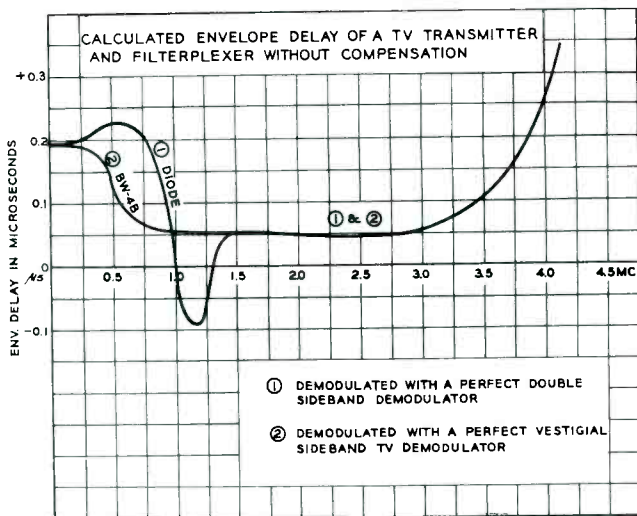


Fig. 7 - Calculated envelope delay of TV transmitter and filterplexer without phase compensation.

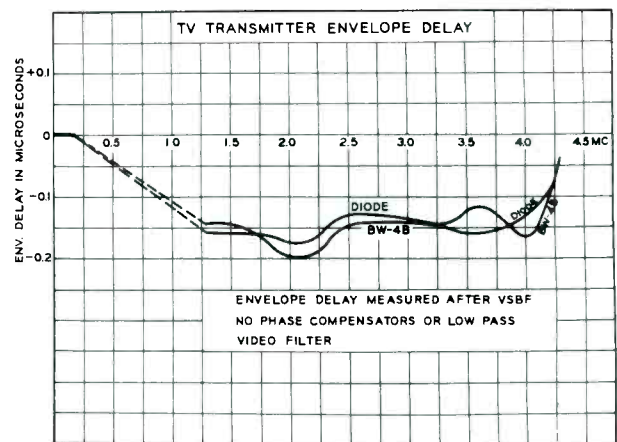


Fig. 9 - Measured uncompensated TV transmitter envelope delay at output of sideband filter using both diode and vestigial demodulators.

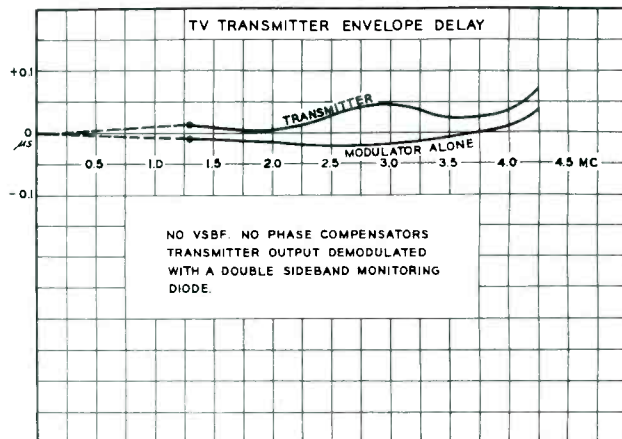


Fig. 8 - Measured envelope delay of TV transmitter visual modulator and overall transmitter characteristic.

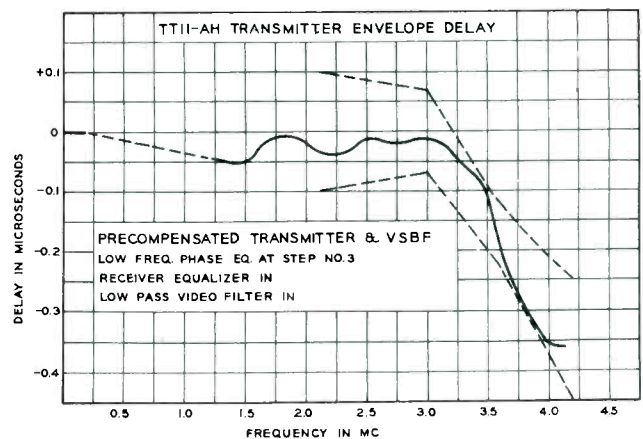


Fig. 10 - Measured envelope delay characteristic of RCA TT-11AH transmitter.

REACTIVATION OF IMAGE ORTHICONS  
UNDER LOW TEMPERATURES

Benjamin Wolfe - Chief Engineer, WJZ-TV  
Westinghouse Broadcasting Co. Inc., ( Md. )  
Baltimore, Maryland.

During October, 1957 our station was interested in observing Russia's Sputnik No. 1. It was desired to make this pick-up so that a film could be made off of our kinescope and this film integrated in a program originating at WBZ in Boston. A very low noise image orth had to be used and the inventor of the "Lumicon", was contacted. Mr. R. Sturm, the inventor, agreed to use the "Lumicon" for this pick-up. The "Lumicon" is similar to the 5820 image orthicon and it was observed that it was transported in dry ice. A study was made of the publication available relative to the effect these low temperatures would have on image orthicons.

The effects of varying ambient temperature upon the performance of an image orthicon have been evident since the beginning of image orth cameras.

While all of us use image orths the thought occurred to rest an image orth at zero degrees F to restrict molecular movement by some degree and see if we could not obtain a signal to noise ratio similar to the "Lumicon". However, it was not until August 1958 that the first tube was observed after being held at approximately zero degrees F for 3 weeks. The effect noted on this particular tube, which had been in use for 970 hours, was not so much the low noise level of the tube, which incidentally was apparent, but the apparent reactivation of the target. Although the tube was originally discarded for excessive sticking and no useable target, this tube gave another 170 hours of operation with extremely low noise and good target control.

At this point it was decided to run further experiments with discarded image orthicons and accordingly a Westinghouse Model CSM-10 Deep Freeze was obtained. This is a 10 cubic foot unit. We are at present storing 32 image orths for a minimum period of 50 days at zero degrees F. Our second tube which had 1100 hours and no target was "Deep Frozen" for 50 days and returned to service. To date it has logged an additional 269 hours before being returned to the deep freeze.

It appears that the tube should rest for at least 50 or 60 days in the deep freeze before returning it to active service, but additional frozen storage time should not hurt the tube.

The following statistics are based on the observation of 32 tubes out of a total of 45 available. The 13 tubes not included are those still in storage at this writing as well as those which were not much improved by cold storage. Twenty-five of the 32 are tubes at WJZ, 5 at KDKA Pittsburgh and 2 at WBZ Boston. Of these 25 at WJZ, 22 have been through the freezing process once and three have gone through twice.

The accompanying chart shows a representative sample of the results. Listed vertically along the left hand edge are the respective serial numbers of the tubes and horizontally along the top are plotted total filament hours. The first shaded area starting from the left of the bar chart shows the total time on the respective tubes prior to being placed in cold storage. The dotted area indicates the added hours of use after being removed and again placed in service. The cross hatched area on the last 3 bars shows the number of hours received after the second freezing.

There seems to be no correlation between the length of time spent in cold storage and the number of hours of added useage, other than the fact that the best results were obtained from tubes that had rested 90 days or longer. The rapidity with which a tube can be brought up to operating temperature is another question that seems to have no concrete answer. Most of the tubes are allowed to come to room temperature before placing them in service. One tube was placed in the camera immediately upon being taken out of the freezer. This particular tube then developed what appeared to be the granddaddy of all ion spots and had to be discarded. This particular method of defrosting has not been tried since, although there may be some merit in pursuing it further.

The greatest number of hours of total life we have gotten thus far is 1452 from Orth serial S-7064. This tube was used 1198 hours initially and again for 254 hours after a 5 month rest. It was removed from service and again placed in storage on 5.20.59. We have not tried it again since that time. The least number of hours received was 465 of which 373 were original and a bonus of only 92 added after a rest of approximately 2 months. This tube however, was extremely noisy and remained so throughout its life and did not respond in the manner of the others.

It should be noted that all times quoted are filament hours and that generally the beam is left up during standby periods. During these times the lens is capped or the turret cocked. The initial times listed were obtained, for the most part, without the use of orbiters and the tubes removed because of excessive sticking, noise or loss of target.

The comments of Mr. Rodgers of KDKA are as follows:-

"The first two tubes tested were quite successful with 625.8 and 574.2 additional hours received after freezing. These two have now been put back in the deep freeze. The third tube is so persistent we are unable to use it. The fourth tube has been tested and has not been put into service in a camera, but is useable. The fifth tube is not useable, primarily because of extremely bad persistency and a microphonic condition.

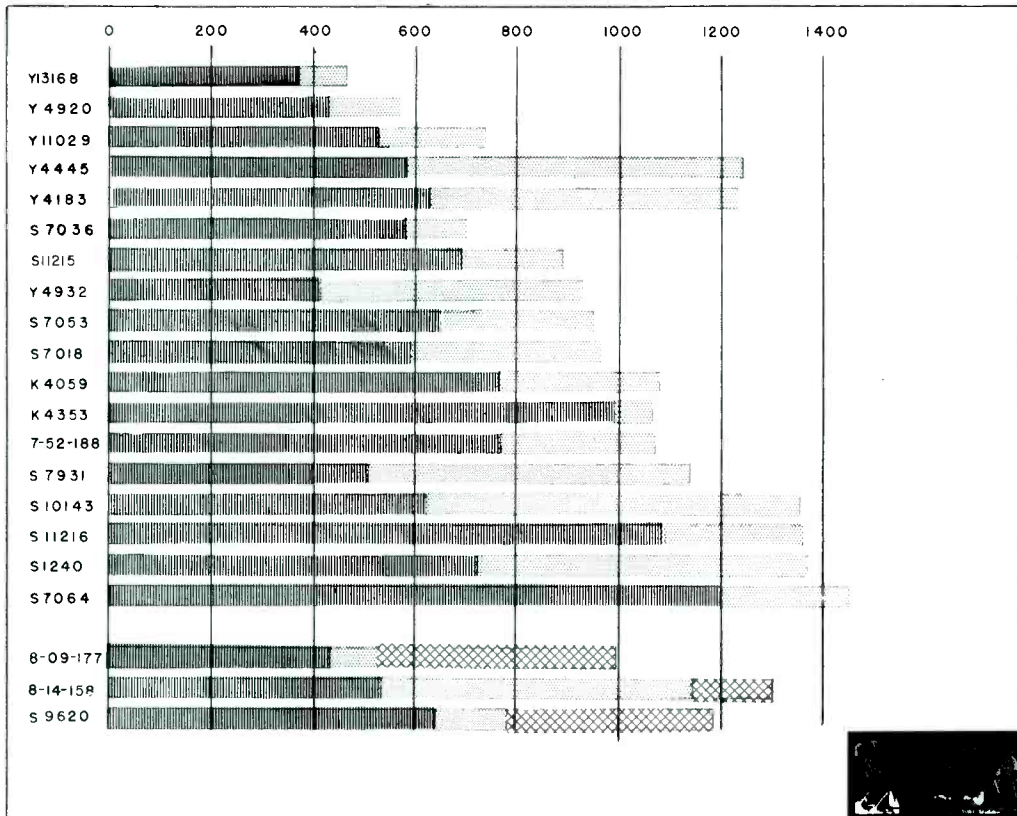
We have observed in all cases that the noise level in the tube becomes very low, as you have already experienced, as a result of being stored in a deep freeze for a period of approximately 60 days. The two tubes which had a successful treatment in the deep freeze and have been used, appear to have the rate at which persistency increases, reduced by a considerable amount. In fact, the operating personnel feel that these two tubes had very little increase in

persistency after being taken from the deep freeze. There are some operating technicians who feel they did not show any increase in persistency during this time. Whether or not this condition is true in all cases, we of course have not had sufficient experience to be able to determine. The other two tubes are so badly persistent that they are not airworthy and we would not be able to determine anything from these two tubes."

And that gentlemen is it - we make no claims for the reasons involved, but do believe we are getting extra hours out of tubes by placing them in cold storage. This we believe exceeds that which can be achieved by the rotation of tubes stored at room temperature.

It might be well to add at this point that some of these bonus hours were not too easily achieved. Some of these tubes, while still exhibiting good S/N ratio, began to stick rather badly, and only by staying away from dark scenes, low key lighting etc, were some of the extremes obtained. Finally, we are not physicists and we wouldn't know how to begin to build an image orthicon. But of one thing we are sure; last year we didn't buy as many tubes.

In closing the writer wishes to thank Mr. Glenn Lahman, Assistant Chief Engineer, for his assistance in this project.



## SOME COLOR SLIDE AND COLOR TELEVISION EXPERIMENTS USING THE LAND TECHNIQUE

Wm. L. Hughes

In several recent articles, Dr. Edwin H. Land<sup>1, 2, 3</sup> has pointed out some fascinating features of color vision which show promise of having considerable effect on commercial color processes of all kinds. It is the purpose of this paper to discuss some interesting results which came of repeating and expanding one small section of Dr. Land's experiments. In particular, we shall be concerned with color pictures produced in the following manner. Two original negatives were taken with relatively narrow band color filters, in particular red and green. These pictures were then displayed both by optical projection and through the use of an intermediate color television system. When optical projection was used, one light source was white (3200°K) and the other light source was either red, green, or blue. When a color television system was used, one of the picture negatives was used to apply identical signals to all three guns of a tri-color display and the system was balanced at Illuminant C. The other picture negative was used to obtain a signal that was added to only one of the color guns. These experiments lead to the conclusion that for this small part of the Land experiments at least, the Land Phenomenon follows a rule of complements which fall in approximately the same order as they do on a C. I. E. color chart. This means that even though the Land Phenomenon is not in any sense explainable from classical additive colorimetric theory, certain aspects of it are nevertheless predictable through the use of a standard color chart.

### Color Slide Experiments

Let us begin in the manner of Dr. Land by making two black and white slides of a colored scene. One of the slides is made from a negative exposed through a green filter (Wratten 58) and the other is made from a negative exposed through a red filter (Wratten 25). Two sets of such slides are shown in Figures 1(a), 1(b), 2(a), and 2 (b). For the moment, let us concentrate on slide set 1(a) and 1(b). In the original scene, the apple is

a bright red, the flowers on the potted plant are a slightly less saturated red, the leaves are green, the ears of corn are bright yellow, and so on. Now let us place the two slides in two identical projectors, placing a green filter in front of the "green" slide and a red filter in front of the "red" slide. If the two images are carefully registered on the screen, the full gamut of colors from red through yellow to green is observed as would be expected since this is simply the old classical two color separation system. No whites, grays, blues, cyans, or magentas are observed as would be expected from classical theory. Now let us remove the green filter and replace it with a neutral density filter which simply reduces the intensity of white light. The new result is quite interesting. The apple and flowers are bright red as before. The corn is definitely not as yellow as before and takes on somewhat of a pinkish cast. The leaves, however, are a rather bluish green, and this color should not appear at all from classical theory. Next, let us remove the red filter and place it on the other projector. The apple immediately turns to a bright, saturated bluish cyan. This happens in spite of the fact that the two light sources are white and red. At this point, classical additive colorimetric theory has completely collapsed. It does not follow at all, however, that classical ideas of color complements (which can be extracted from a C. I. E. color chart) have also collapsed. Oddly enough, just the opposite appears to be true.

Before discussing these statements in more detail, however, it is interesting to reconsider some of the interesting work done on color vision by D. L. MacAdam and his colleagues at the Eastman Kodak Research Laboratories. In particular, let us recall a paper entitled Color Balance for Television which appeared in the January, 1955 proceedings of the Institute of Radio Engineers. This paper reviewed some of the opinions reached by MacAdam as well as by Evans,<sup>4,5</sup> Brewer,<sup>5,6</sup> and others. These opinions expand on classical theory roughly as follows. Classically, the eye seems to



Figure 1a.



Figure 1b.



Figure 2a.



Figure 2b.

behave as though it has three receptors to which we like to assign the colors red, green, and blue. Carefully note that the description is "as the eye seems to be". The actual mechanism of color vision is probably far different, of course. Quantitative colorimetric theory is built on the premise that all colors are described by linear combinations of stimulation of these three perceptors. The thing brought out by MacAdam, Evans, Brewer, and others is that there is an additional adaption phenomenon which appears to act something like three automatic gain control systems. There is one automatic gain control for each perceptor, and they operate simultaneously. What this means is that when the average quantity of red light from a scene increases, the eye's red gain decreased, thereby making an area that is pink to a spectrophotometer seem more white to the eye. Apparent colors will then distribute themselves around the eye's new reference white in approximately the same order as they would be distributed around a "true" white on a C.I.E. color chart. A similar effect would be noted regardless of the direction in which there was an average light increase. The eye and the mind would adapt to the new situation and make the average light seem more white than it really is. This adaptive characteristic is really very desirable. For example, it keeps faces from appearing blue under fluorescent light and red under incandescent light and keeps ordinary objects from changing color as the spectral characteristics of daylight change.

With this information on adaptation, let us return to our experiment with white and red light sources which are used to project our two original "red" and "green" slides. Consider Figure 3 in which two such light sources are plotted on a standard C.I.E. color chart. (Theoretically, we have no right to use such a chart for this purpose, but we are going to do it anyway.) A reference white somewhere between a home projector (3200°K) and color television (illuminant C) is chosen for illustrative purposes. We shall come back to the choice of reference whites a little later. Theoretically, all points on the picture should fall on the solid line segment  $\overline{abc}$ . A spectrophotometer would insist that they do, but our eye tells us they do not. Regardless of what other colors appear in the picture, some points have the appearance of occurring either along or in the

vicinity of the dotted segment  $\overline{cd}$ . We can never be really sure of anything but their general location, of course, because the result is completely subjective. Until we know and understand the spectral and spatial transfer function of the eye to the mind, we must be content with speculation. It is encouraging, however, when speculative effects become predictable prior to the experiment.

Now let us consider the possible adaptive phenomena when the red filter is placed in front of the "red" projector. The average light may fall around point  $b$  on Figure 3. Anything that is bright red will still be on the red side of point  $b$  and will therefore still be red. Anything that is less red, however, will be on the other side of the average point and might well appear bluish cyan. That is, it might seem as though it is located towards point  $d$ . If we now place the red filter over the "green" projector, we have probably done very little to shift the spectral char-

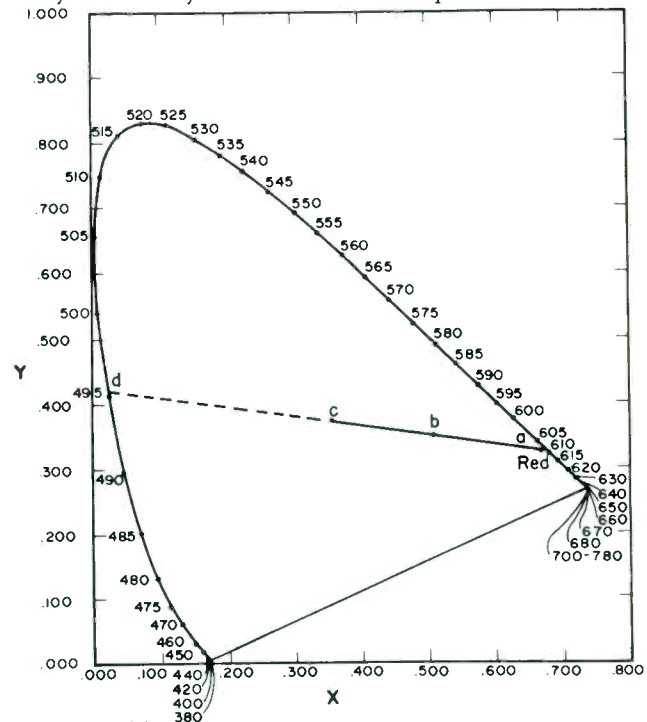


Figure 3.

acteristics of the average light. However, anything that was previously a bright, saturated red will be less red than anything else in the picture. If there is anything to the adaptive phenomenon, it should turn a bluish cyan. That is, it should seem to the eye that it has shifted a long way towards point d in Figure 3. This, of course, is precisely what happened in the first experiment.

Now let us make some predictions on this basis. If there is anything to this postulated association between the Land Phenomenon and the adaptive phenomenon, we should be able to place any colored filter over either projector and predict the color of the apple. The following predictions should hold.

1. a red filter on the "red" projector should yield a red apple
2. a red filter on the "green" projector should yield a bluish cyan apple
3. a green filter on the "red" projector should yield a green apple
4. a green filter on the "green" projector should yield a magenta apple, not a red apple
5. a blue filter on the "red" projector should yield a blue apple
6. a blue filter on the "green" projector should yield a greenish yellow apple.

Experiments with a No. 25 red Wratten, a No. 47B blue Wratten, and a No. 58 green Wratten will show that all of these predictions hold extremely well. Further, the larger the different

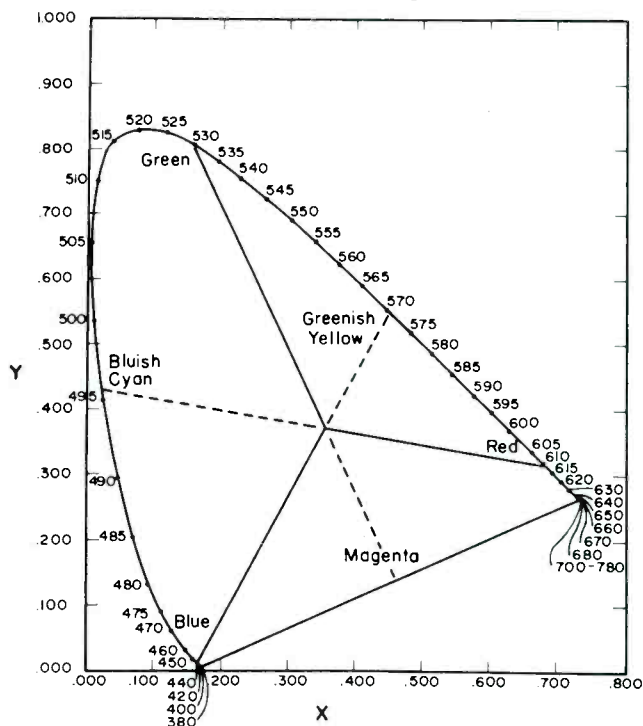


Figure 4.

color areas become, the less pronounced is the effect. This is, of course, what would be expected in an adaptive phenomenon. Predictions 1 and 2 are shown, of course, on Figure 3. Figure 4 shows the axes of predictions 1 through 6. Further, similar experiments (to be described shortly) with a color television system yield essentially the same results.

Now let us return to the question of reference whites. Consider the sets of axes of Figure 5. The solid axes correspond to the complete axes of Figure 4 except that the reference white is 3200 degrees Kelvin. This corresponds to the typical incandescent projector. The dotted axes of Figure 5 also correspond to the complete axes of Figure 4 except that the reference white is illuminant C. It will be noted that the possible ranges of saturated bluish cyans and greenish yellows are less than ten millimicrons in both cases. The range of magentas cannot, of course, be evaluated in this way.

Despite the fact that there is less than a ten millimicron variation in the bluish-cyans and greenish yellows, a strong objection can well be raised at this point. The upper wavelength projection of the so called bluish-cyans geometrically falls around 502 millimicrons which is definitely more cyan than bluish. The lower projection, which is around 491 millimicrons, is definitely bluish. In the greenish-yellow range, the lower projection is about 568 millimicrons which is distinctly greenish yellow. The upper projection which is around 575 millimicrons, is definitely on the yellow side. We can only hope to define general regions of the color chart because no existing photosensitive instrument can measure the proper

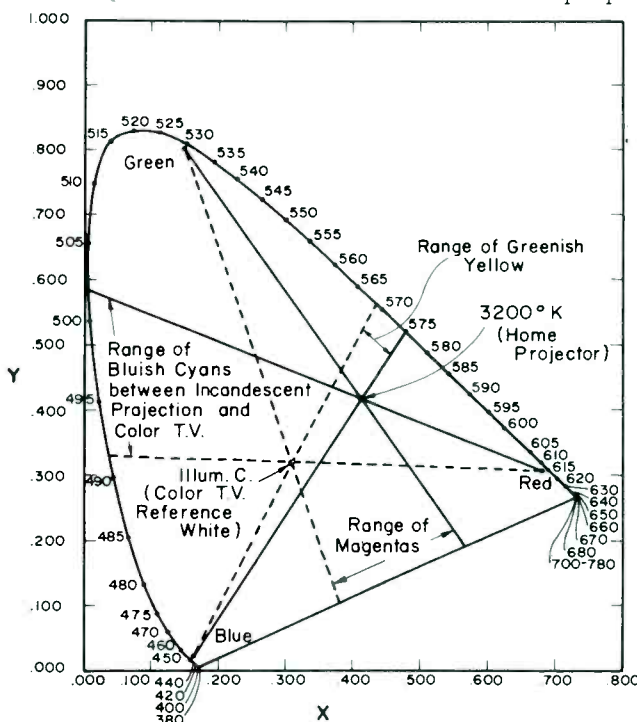


Figure 5.

point for us. Further, when a red filter is placed on the "green" projector, the range of bluish-cyans available is definitely a function of the intensity of the "red" projector which is putting out 3200 degrees Kelvin light. The more this projector is stopped down, the more bluish and less cyan the normally red subjects become. Similarly, if a blue filter is placed on the "green" projector, the greenish-yellow color of normally red objects is a function of the intensity of the "red" projector which is still really just 3200 degrees Kelvin. The less intense the "red" projector becomes, the more yellowish and less greenish the normally red objects become. This is undoubtedly part of the reason why more colors than just one axis on the color chart are often observed in the Land Phenomenon.

All this brings up the question of the validity of using a C.I.E. chart in the first place. This practice is open to severe question because the complement extreme colors are subjectively simulated by the eye and the mind. They do not correspond to a spectral characteristic normally associated with a point on the chart. However, in the sense that we habitually (though sometimes apparently incorrectly) associate certain ranges of colors with certain areas on the chart, it is useful in predicting qualitative visible results of the Land Phenomenon. Right or wrong, that is the reason for its use. It might be possible to set up some elaborate color matching experiments to check the idea more quantitatively, particularly since Dr. Land's work does indicate that two color domains can be observed simultaneously. This writer, however, is not clear on just how to go about it. What is actually done here is to qualitatively modify colorimetric theory by tacitly accepting the idea of three perceptors with individual automatic gain controls. The C.I.E. chart, as originally derived, assumes that the eye acts as a tri-sensitive linear device. The addition of automatic gain controls would not invalidate its use if we could quantitatively evaluate the gain shifts. If more complex facets of color make the three channel automatically gain controlled model of vision incorrect too often, it may be better to abandon the chart entirely.

#### Color Television Experiments

Certain additional experiments were definitely called for as an adjunct to those preceding. First, it seemed expedient to examine the Land Phenomenon with movement in the pictures. Second, it was desirable to be able to mask certain areas of the picture to assure ourselves that some additional unforeseen phenomenon was not causing the observed results. A color television system is an ideal way to examine these things. Iowa State University has an operating color television system which can be made to utilize color separations on a two image strip of 35 millimeter black and white film. Further, a movie camera was already in existence to make film for this color television system. The amount of work necessary to convert the entire system to utilize the Land Phenomenon consisted of changing camera filters, changing a few cables in the color television sys-

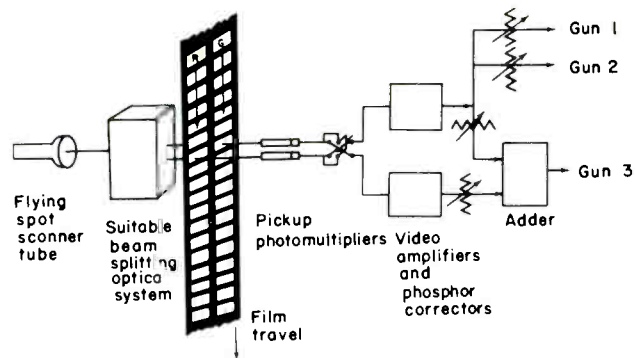


Figure 6.

tem, and clipping a few strategic points together in the video matrix system. The entire system is symbolically illustrated in Figure 6. Provision was made to feed a signal from one of the film tracks to all three guns of a 21 inch shadow mask and to the three tubes of a triniscope. In addition, it was possible to add a signal from the other film track to any one gun of the shadow mask or any one tube of the triniscope.

Several hundred feet of plus X panchromatic film were shot and developed to a gamma approximately the inverse of that of the cathode ray tubes. The film gamma was controlled on the reproducibility of a gray scale shot with the original camera under typical scene flat lighting. This gamma was compared with the video signal in the scanner. In this way, scattering in both the film camera and flying spot scanner optics was accounted for. One of the film tracks was used to control all three color channels equally so that a simple black and white picture was produced from it. The signal from the other film track was then added to one of the three color channels in varying amounts. The usual white balance was around illuminant C when only one film track (that controlling all three guns) was on. Other white balance positions on the color chart were occasionally used, however. Various types of colors and motions were incorporated in the films.

The conclusions of the color television experiments are as follows. Every phenomenon observed with the projected slides was observed with the color television system, although it was generally more difficult to get saturated colors on television. Motion appears to have no detrimental effect on the observed colors unless it is so fast that the color is irrelevant anyway. There was no indication that the degradation observed with fast motion is any worse than it would be with any other type of color system under similar circumstances. Strategic masking of various sections of the picture merely served to prove that the observed color in a small area was definitely a function of the surrounding area. When all but small areas were masked, they returned to essentially the colors that would be predicted by classical colorimetric theory. Actually, because of the scattered light in the color displays, the following could be observed. A gray or blue object in the picture would turn blue when the red signal was turned up. However, when all of the picture but that object was masked

with a piece of cardboard, the object simply turned more reddish with the application of an increased red signal. This light scattering probably accounts for the difficulty encountered in getting really saturated colors when the color television system is operated in the manner called for by the Land technique.

One additional phenomenon was observed. The color "A. G. C. system" of the eye apparently has a finite transient. For example, suppose the red filter is placed over the "green projector" so that the apple is appearing bluish cyan. If the filter is suddenly removed, the apple will momentarily appear red before returning to a neutral gray. This has formerly been referred to as "fatigue", but it does not require long observation of the complementary color and it does exhibit the characteristics of a transient overshoot in a servo system. It also occurs for all colors. If the blue filter is suddenly removed from the "red projector", the apple will go from blue to greenish yellow to neutral, the whole process taking less than a second after the filter is removed.

#### Discussion

General conclusions in a subject such as this are extremely hazardous. The writer would like timidly to offer a few, however.

1. In all probability, full color projection and color television are and will remain three dimensional mediums. This seems likely not only from these experiments but also from fundamental information theory ideas which have nothing to do with the eye and the mind. For example, certain yellow and white colors could be made to stimulate the red and green records in an exactly similar fashion. Thus it would be impossible to tell the difference between these particular yellows and whites. Further, a saturated, fairly narrow band blue would not stimulate either a green or red record. Thus it would be impossible to tell the difference between this blue and black. This doesn't mean at all that the two dimensional system couldn't produce a blue, black, or yellow. It simply is not apt to be too faithful to the original scene. Other irregularities can be postulated in a similar fashion.

2. It is unquestionably true, however, that only two dimensions can go far beyond what the old classical theory is willing to allow. Complementary colors are simulated by the eye and the mind with absolutely no difficulty or hesitancy. Variations of intensity also have the effect of

shifting observed colors above or below a color complement axis, not only along the axis. This latter effect is much less pronounced, but nevertheless seems to be unquestionably present.

3. The standard C.I.E. color chart, though derived from classical colorimetric theory, is nevertheless useful in predicting the general trend of colors that will appear in the Land Phenomenon.

4. One might find it convenient to think of color reproduction as follows. Newton, Maxwell, and others have given us first order terms of the equations of color vision. Drs. Evans, MacAdam, Brewer, and Land have apparently done two things. They have given us second order terms and have illustrated very beautifully that, in many cases, these second order terms are as important as the first order terms.

5. The concept of color vision as three perceptors with automatic gain controls is a rather good model for many purposes, and is consistent with many of the phenomena observed by Dr. Land.

The writer would like to point out that only one very small section of Dr. Land's broad gamut of experiments are considered in this paper, and that no pretense is made that the broader aspects have been fully investigated.

The writer would like to thank Mr. L. A. Facto of the Iowa State University Information Service for his permission to use the slides he made in his own experiments on the Land Phenomenon. These slides are those illustrated in Figures 1 and 2 of this paper.

#### Selected References

1. Land, Edwin H., Experiments in Color Vision, Scientific American, pages 84-99, May, 1959.
2. Land, Edwin H., Color Vision and the Natural Image, Part I, Proceedings of the National Academy of Sciences, pages 115-129, January, 1959.
3. Land, Edwin H., Color Vision and the Natural Image, Part II, Proceedings of the National Academy of Sciences, pages 636-644, April, 1959.
4. Evans, R. M., On Some Aspects of White, Gray, and Black, Journal, Optical Society of America, Vol. 39, pages 774-779, 1949.
5. Evans, R. M., and Brewer, W. L., Observer Adaptation Requirements in Color Photography and Color Television, Journal, Society Motion Picture and Television Engineers, Vol. 63, pages 5-9, 1954.
6. Brewer, W. L., Fundamental Response Functions and Binocular Color Matching, Journal, Optical Society of America, Vol. 44, pages 207-212, 1954.

DESIGN AND PERFORMANCE MEASUREMENTS  
ON A NEW ANTI-FADE ANTENNA  
FOR RADIO STATION WOAI

Charles L. Jeffers  
Southland Industries, Inc.  
San Antonio, Texas  
And  
Stephen W. Kershner  
A. D. Ring & Associates  
Washington, D.C.

Summary

A new anti-fade type radiator for Station WOAI is described. Vertical radiation patterns are presented on the basis of computations from predicted current distributions. Measurements on a model antenna generally confirm the performance predicted by the computations. Skywave measurements using pulse techniques were made on the full scale antenna to determine the optimum tuning and the suppression of skywave signals. These measurements show skywave signals transmitted by both the E and F layers of the ionosphere. Final performance data are presented, including current distribution measurements, the vertical radiation pattern and groundwave field intensity measurements.

Manuscript

Radio Station WOAI is authorized by the Federal Communications Commission to operate in San Antonio, Texas, on the clear channel frequency of 1200 kc with a power of 50 kw unlimited time. Both groundwave and skywave signals are protected from interference from other stations. The most efficient use of the assignment requires maximum groundwave signal during daytime hours. During nighttime hours, the groundwave signal should be free from selective fading out to the distance where the signal is just adequate to overcome noise, then the skywave signal should rise rapidly so as to provide maximum secondary service. These requirements call for an antenna having a carefully controlled vertical radiation pattern.

In April, 1956, the WOAI antenna tower was struck by an Air Force plane, and plans were made for installing a new antenna of optimum design at a location creating less air hazard. A new transmitter site was selected some 17 miles

southeast of San Antonio, and a location for the tower was chosen some 3,000 feet from the 1531-foot tower which supports the television antennas of WOAI-TV and KENS-TV.

Several workers, including one of the authors, have reported on various aspects of anti-fade antennas for broadcasting applications.<sup>1-6</sup> A new type of anti-fade antenna was reported by Jeffers in 1948<sup>3</sup>, but in view of recent advances in the knowledge of antenna performance, it was decided to reexamine the possibilities.

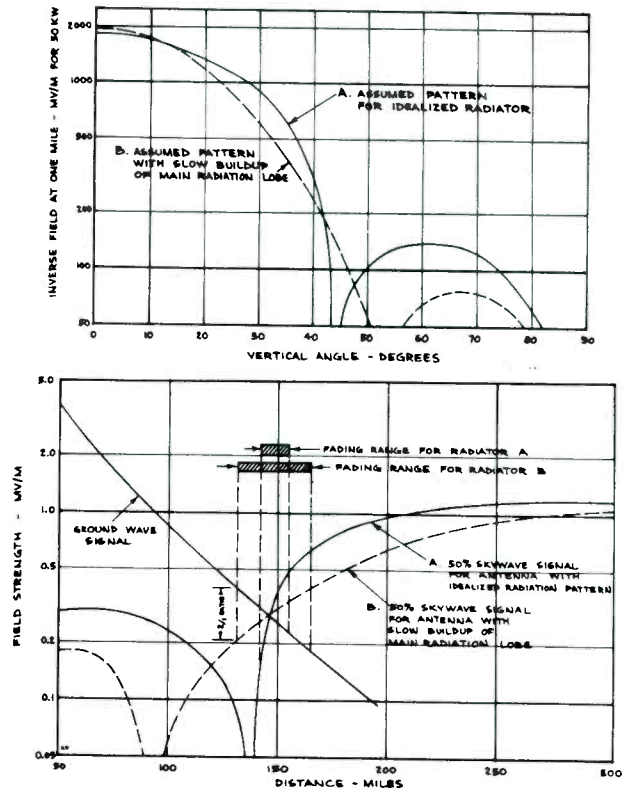


FIGURE 1. VERTICAL RADIATION PATTERN AND SKYWAVE SIGNAL FOR IDEALIZED RADIATOR

## DESIGN CONSIDERATIONS

The first task was to undertake to outline in general terms the radiation pattern requirements for providing optimum nighttime service. Figure 1 shows vertical radiation patterns and signal vs. distance curves for two assumed radiators. The solid lines represent the performance obtained from an idealized radiator, and the dashed lines illustrate an antenna with less desirable characteristics.

In the zone where the groundwave and skywave signals are of approximately the same intensity, rapid or selective fading will occur. Periodic cancellation of the carrier signal takes place, creating the effect of over-modulation and causing serious distortion. For optimum design this fading zone should occur just beyond the limits of useful groundwave service as limited by noise. Furthermore, the skywave signal should increase rapidly with distance as shown by Curve A, Fig. 1. Curve B shows that a slow build-up of skywave signal is undesirable as it results in a wider fading zone. Also, the suppression of skywave signals at closer distances as influenced by high angle lobes must be adequate to prevent an extension of the fading zone. These factors necessitate a vertical radiation pattern tailored to the frequency of operation, ground conductivity and minimum field strength for satisfactory groundwave service.

Figure 2 shows the vertical radiation patterns for three types of radiators. These patterns were computed on the basis of the simple sinusoidal current distributions shown, with the phase velocity assumed equal to the velocity of light. Pattern A is for a con-

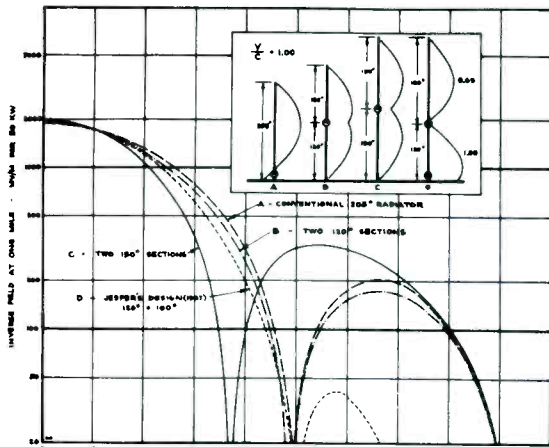


FIGURE 2. VERTICAL RADIATION PATTERNS BASED ON SIMPLE SINUSOIDAL CURRENT DISTRIBUTION

ventional base-fed radiator with a height of  $205^\circ$ . Patterns B and C are for sectionalized antennas insulated at the center with current distributions as shown. Pattern D is for the sectionalized antenna designed by Jeffers in 1947. This design results in almost complete suppression of the high angle radiation. Patterns A, B and D have very nearly the desired characteristics for the WOAI application. It is well known, however, that the current distribution in an actual antenna of practical dimensions does not correspond closely to the assumed simple sinusoidal current distribution. An investigation of radiation patterns based on practical current distributions was therefore undertaken.

Figure 3 shows the predicted current distribution for four types of radiators. The prediction of current distribution was based on a modification and extension of a method outlined by Schelkunoff and Friis<sup>7</sup> for determining the approximate current distribution of cylindrical radiators of anti-resonant length. The total current  $I_0$  is composed of an  $I'$  "in phase" component and a quadrature component,  $I''$ . The  $I'$  component may be thought of as representing the power component of the current, while the quadrature component is responsible for most of the radiation from the antenna. The constant  $k_1$  is simply the ratio  $I'_{max}/I_{max}$  and the constant  $\gamma$  is the ratio of the velocity of the radiator to the phase velocity on the radiator.

The constants  $k_1$  and  $\gamma$  were determined by reference to base impedances for cylindrical antennas of anti-resonant length. Complete details, including equations, for obtaining the current distributions are given in the Appendix.

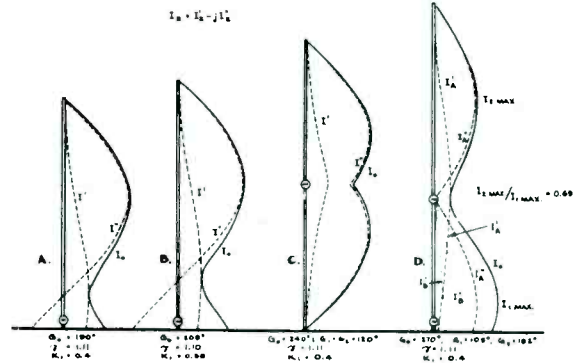


FIGURE 3. PREDICTED CURRENT DISTRIBUTION (AFTER SCHELKUNOFF)

The method used to predict the current distributions is reasonably simple and provides an adequate approximation for this application. It should be noted that considerable information is available concerning more advanced methods of establishing the current distribution of cylindrical radiators,<sup>8,9,10</sup> but unfortunately the methods which yield the most accurate results are quite complex and require tedious computations.

Current distributions A and B of Figure 3 show that the minimum of the current distribution is filled in by the in-phase component of current. The amount of the fill increases as the effective diameter of the radiator is increased.

Current distribution C of Figure 3 is based on the assumption that both the in-phase and quadrature components of current will be symmetrical with respect to the sectionalizing level, where power is applied. Such symmetrical current distribution would be expected if the radiator were removed from the ground plane; thus it is apparent that the effect of the ground plane on the current distribution has been neglected.

Current distribution D shows the predicted current distribution for the Jeffers antenna. The length of the upper section length was adjusted to be anti-resonant, and the current predicted for the bottom section is based on two sets of components as indicated. Components  $I_B^I$  and  $I_B^{II}$  are predicted in the same manner as for the simple base-fed radiator. The sum of these components provides the total current and the desired loop current ratios.

Figure 4A shows the vertical radiation patterns for three types of antennas computed on the basis of the predicted current distributions shown by Figure 3. All vertical patterns presented are based on the usual assumption of a flat infinitely conducting ground plane and the details, including the equations used, are given in the Appendix. Note the large amount of null fill in the A and B patterns for conventional base-fed radiators. The relatively large amount of high angle radiation obviously makes this type antenna unsuitable for anti-fade applications.

Pattern C has the desired characteristics for the WOAI application, and Pattern D also exhibits desirable characteristics with very effective suppression of high angle radiation.

Figure 4B shows the predicted WOAI groundwave and 50 percent skywave signals computed for antennas providing the vertical patterns shown by Figure 4A. The skywave signals are based on the "latitude" 50% skywave curves developed for the clear channel hearing at the FCC. The skywave signals shown for the conventional base-fed radiators are undesirable because of inadequate close-in suppression of the skywave signal. The Jeffers antenna provides the best suppression of close-in skywave signal, but the build-up of the skywave signal in a range from 125 to 175 miles is relatively slow, and undesirable, as it increases the depth of the fading zone.

The antenna consisting of two 120° sections was selected as the optimum design because of the rapid build-up of skywave signal between 125 and 175 miles. While the close-in skywave suppression is not as good as the Jeffers antenna, it is still considered adequate. Consideration of the several vertical patterns explored shows that the desired rapid build-up of

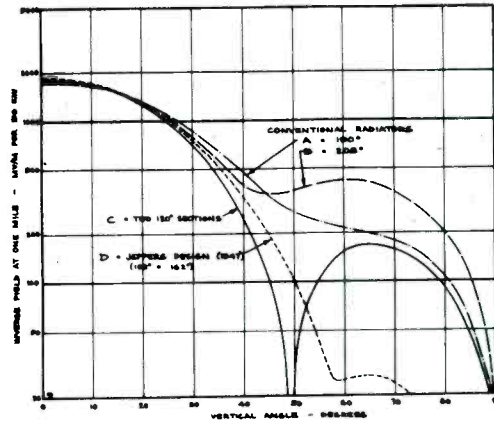


FIGURE 4A. VERTICAL RADIATION PATTERNS BASED ON PREDICTED CURRENT DISTRIBUTION (AFTER SCHUNKOFF)

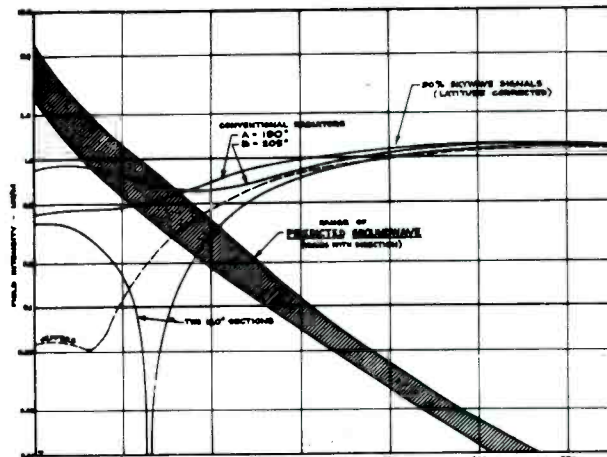


FIGURE 4B. PREDICTED GROUNDWAVE AND SKYWAVE SIGNALS

skywave signal in the region of the fading zone can be obtained only with an antenna having a sharp null in the vertical pattern and a high angle lobe of appreciable size.

### MODEL TESTS

A model of the proposed antenna was constructed to permit a further evaluation of the performance. Figure 5 is a sketch of the model antenna as scaled for measurements at a frequency of 755 mc. The model was constructed of 1/8 inch brass tubing with insulated spacers provided as indicated. A miniature coaxial line was used to transfer power to the sectionalizing insulator. The outer conductor of the coaxial line was insulated from the lower section of the antenna as indicated, and the position of the shorting plug was adjusted to obtain the required base isolation.

Figure 6 shows the arrangement of measuring equipment employed to measure the amplitude and phase of the currents on the model antenna. The model was mounted on a copper-covered wall of a special test room, with the wall simulating the ground in the case of the actual antenna. The other surfaces of the room were covered with R.F. absorbing material so as to make an anechoic chamber simulating an infinite ground plane in free space. One miniature balanced shielded sampling loop was employed to sample the current on the antenna, and a second loop was used to obtain a reference signal. Choke coils were used to minimize currents on the sampling lines. The loops were coupled to a receiver through a variable attenuator and a terminated slotted coaxial

line, as shown by Figure 6. One loop was maintained at a fixed position and the other loop was moved along the model antenna to measure the current distribution. At each position the variable attenuator and slotted line probe were adjusted to produce minimum signal at the receiver input. The relative amplitude and phase of the current were then computed as a function of the location of the pick-up probe on the slotted line and the attenuator setting.

Figure 7 shows three sets of current distribution measurements made for three conditions of base tuning. The tuning was accomplished by adding short capacitive stubs of wire just above the base insulator. Analysis of Figure 7 shows that the amplitude of current in the lower element of the antenna can be controlled by base tuning. A completely symmetrical current distribution could not be obtained due to coupling from the image antenna, but the current distribution obtained with the 1.2 centimeter stub is reasonably close to the assumed symmetrical distribution.

Figure 8 shows vertical radiation patterns for the model antenna computed from the current distribution measurements. These patterns were computed by a graphical integration process. The results show that the base tuning may be used to control the angle of minimum radiation. The efficiency figures (inverse field strength at one mile) shown by Figure 8 were determined by integration of the radiation patterns.

Figure 9 shows the 50 percent sky-wave signals based on the vertical radiation patterns computed from the

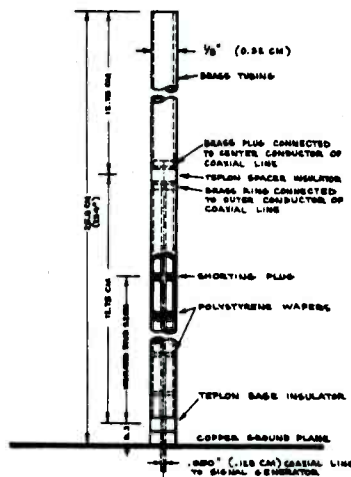


FIGURE 5. SKETCH OF MODEL ANTENNA

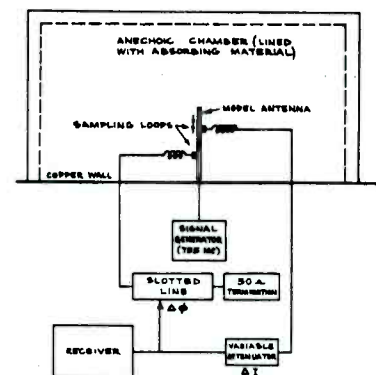


FIGURE 6. TEST EQUIPMENT USED FOR CURRENT DISTRIBUTION MEASUREMENTS

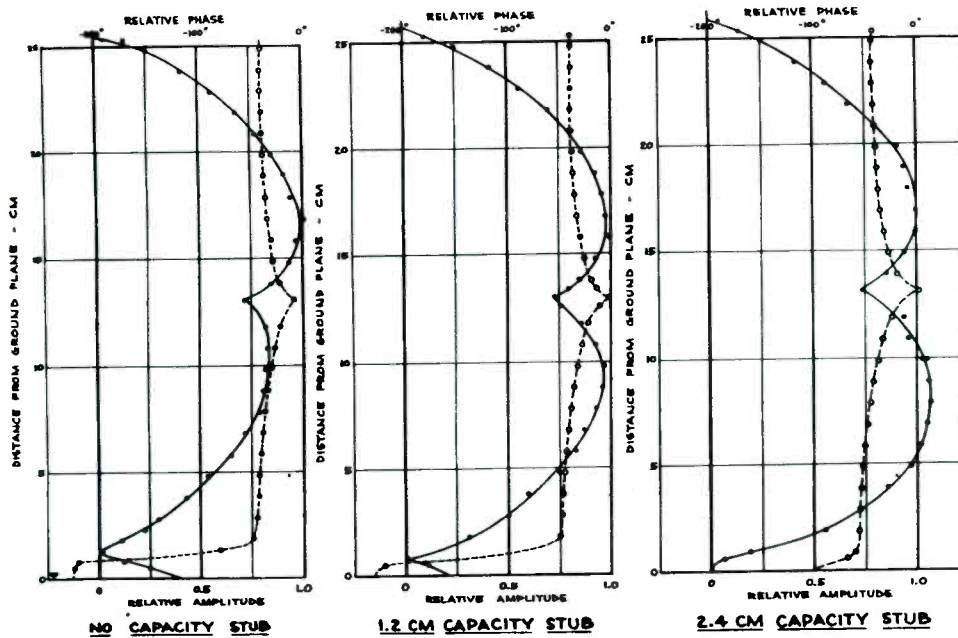


FIGURE 7. CURRENT DISTRIBUTION OBTAINED ON MODEL ANTENNA (755 MC)

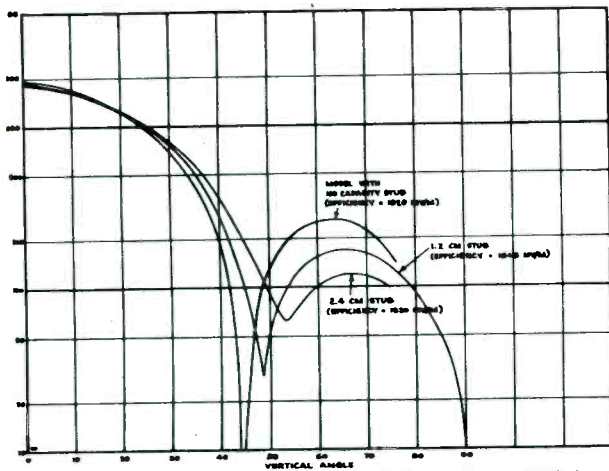


FIGURE 8. VERTICAL RADIATION PATTERNS FOR MODEL ANTENNA AS COMPUTED FROM MEASURED CURRENT DISTRIBUTION

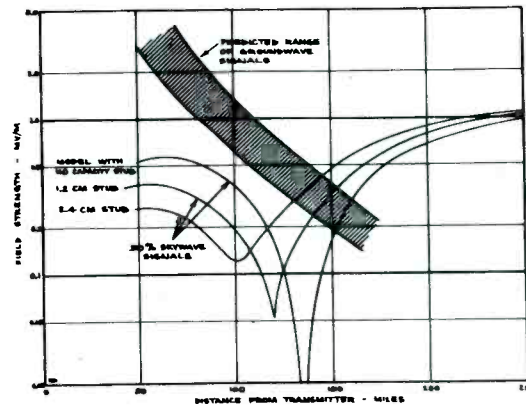


FIGURE 9. GROUNDWAVE AND SKYWAVE SIGNALS PREDICTED FROM MODEL MEASUREMENTS

model measurements. The model with the 1.2 centimeter stub provides the required suppression of high angle skywave signal and exhibits the desired rapid build-up of signal in the region from 125 to 175 miles.

#### ADJUSTMENTS AND PERFORMANCE MEASUREMENTS

Figure 10 is a sketch showing details of the antenna as constructed at the new transmitter site of Station WOAI.

The overall height is 540 feet, or approximately  $240^\circ$ , at 1200 kc. The tower is insulated at the base and at the mid-point, 270 feet above ground level. The tower was manufactured by Stainless, Inc. and is a uniform triangular cross-section guyed structure, with a side dimension of 5 feet. The isolation required at the sectionalizing insulator level and the base is obtained by using insulated stub sections formed by the tower legs and the insulated transmission line and wiring

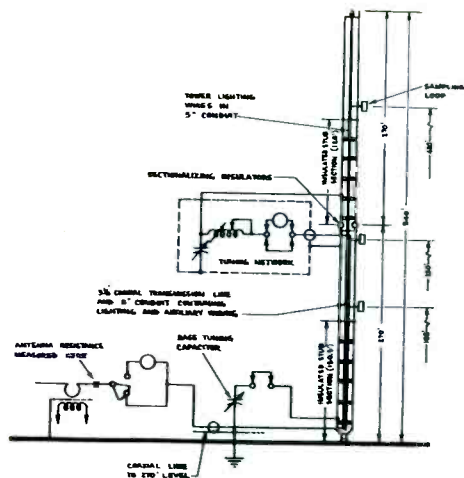


FIGURE 10. DETAILS OF WQAI ANTENNA

conduit. All wiring is housed in a single 5-inch galvanized steel conduit which is centered in the tower cross-section and insulated from the tower where required. The 3-1/8 inch transmission line required to transfer power to the sectionalizing insulator level is attached to the center conduit. An L network is utilized to match the transmission line to the impedance presented across the sectionalizing insulators. The base of the antenna is tuned by a variable capacitor employed in conjunction with the inductive stub section. Three sampling loops are located on the tower as shown by Figure 10 and the coaxial lines from these loops are connected to a phase monitor located at the base.

Figure 11 shows the results of measurements made to determine the effect of base tuning on the groundwave efficiency. Current ratios as provided by the sample loop signals are also shown. Field measurements were made at two clear locations at distances of 2.6 and 5.1 miles, and the results were adjusted for equal power input to the antenna. A base tuning susceptance of 1.4 mmhos provided maximum groundwave efficiency.

Observations of the suppression of sky-wave signals were then made by employing pulse transmissions during the experimental period and observing the results at significant distances. The Continental transmitter of WQAI was modified for pulse operation by keying one of the low-power stages with a pulse generator of special construction. The pulse repetition rate was approximately 200 per second and the width of the pulse was approximately 100 micro-seconds. Observations were made at three locations where the signal was picked up by a wide-

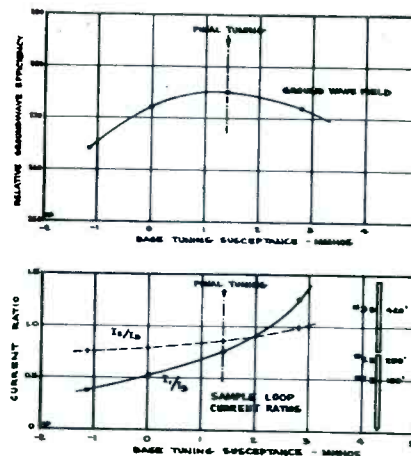


FIGURE 11. GROUND WAVE EFFICIENCY AND SAMPLE LOOP CURRENT RATIOS VS. BASE TUNING SUSCEPTANCE

band receiver and displayed on a Tektronix oscilloscope. A large single-turn loop antenna was used to pick up the signals, as it was believed this type of antenna would offer minimum directivity in the vertical plane.

Figure 12 shows photographs of pulse signals as received near Austin on October 29, 1958. Photograph A shows an F layer pulse with a delay of 1,100 microseconds and two pulses of greater delay which are probably two and three-hop F pulses. The groundwave pulse extends well beyond the lower edge of the photographs. Photograph B shows a small E layer pulse and an F layer pulse. During most of the night, no E layer signals were present, but just before daybreak some weak E layer signals as shown by photograph B were observed.

Figure 13 shows photographs of pulse signals received at Temple. Photograph A shows E layer and F layer pulses along with a weak two-hop E layer pulse. Several other weak pulses are also evident. The interference evident in the groundwave pulse was caused by pickup of R.F. signals generated by the oscilloscope sweep circuits. Photograph B shows the groundwave pulse only with no skywave signals evident. This condition was typical of the night of November 5 when no F layer signals were observed and E layer signals, when observed, were relatively weak.

Figure 14 shows photographs of signals received at Waco on October 28, 1959. Photograph A shows E layer and F layer pulses and photograph B shows one-hop and two-hop E layer pulses and

also an F layer pulse. The one-hop E layer pulse is considerably wider than the transmitted pulse, indicating a considerable spread of effective virtual heights.

Figure 15 shows two unusual conditions observed at Waco. Photograph A shows E layer and F layer pulses followed by several pulses having a large delay. The largest of these pulses has a delay of approximately 2,500 micro-seconds indicating a two-hop F layer mode. Photograph B shows a double pulse with the larger peak occurring at the correct time delay for E layer transmission. The smaller pulse indicates a time delay of 150 micro-seconds corresponding to a virtual height of only 80 km. The interference apparent on Photograph B was caused by an adjacent channel station.

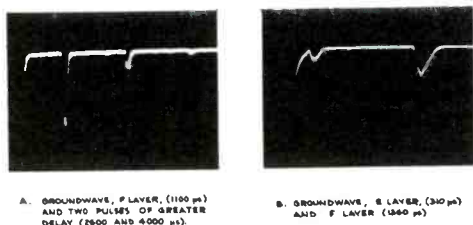


FIGURE 12. PHOTOGRAPHS OF PULSE SIGNALS RECEIVED AT AUSTIN (84 MILES) ON OCTOBER 29, 1958

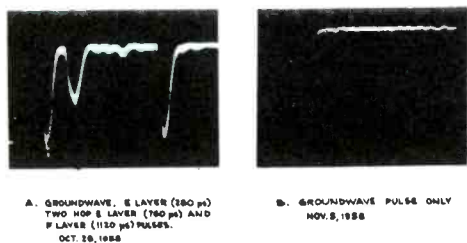


FIGURE 13. PHOTOGRAPHS OF PULSE SIGNALS RECEIVED AT TEMPLE (136 MILES)

Figure 16 shows the results of a time delay analysis of the pulse observations made at the three locations. The observed time delays are plotted as a function of the distance from the transmitter. The experimental data are compared to computed time delay curves based on virtual ionosphere heights of 100 km for E layer transmission and 240 km for F layer transmission. There appears to be little question but what the pulses having the greatest time delay were transmitted by the F layer of the ionosphere.

Figure 17 shows the results of pulse amplitude observations made just north of Austin on the night of October 29, 1958. The base tuning of the antenna was varied and the ratios of skywave to groundwave pulses were observed over a period of approximately two hours. A number of observations were made for each tuning condition and the average results are shown. During most of the night the F layer pulse was the only skywave pulse evident. As day-break approached some weak E layer signals were observed. It was evident from the observations that during most of the time the skywave signals completely penetrated the E layer and were reflected by the F layer. The results show the base tuning for minimum E and F layer signals.

Figure 18 shows the pulse amplitude

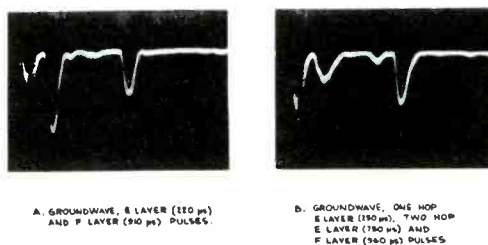


FIGURE 14. PHOTOGRAPHS OF PULSE SIGNALS RECEIVED AT WACO (170 MILES) ON OCTOBER 18, 1958

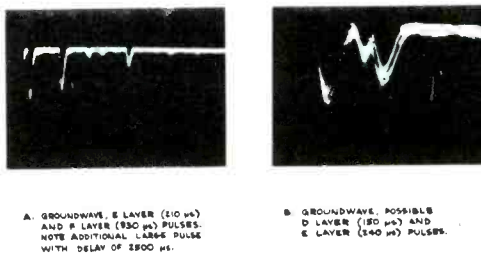


FIGURE 15. PHOTOGRAPHS OF SOME UNUSUAL PULSE SIGNALS RECEIVED AT WACO (170 MILES) ON OCT. 18, 1958

results obtained at a location near Temple, Texas, 135 miles from the transmitter site. Observations were made at this location on two nights as indicated. E layer signals were observed on both occasions, but F layer signals were observed only on the night of October 28. The E layer signal was substantially higher on October 28 than on November 5, but in both cases minimum E layer signal was obtained with a base tuning susceptance of approximately 1.3 mmhos.

Figure 19 shows pulse amplitude results obtained at a location near Waco, Texas, some 170 miles from the transmitter site. E layer signals were observed on October 28 and November 5, and on October 28 F layer signals were also present. The results show minimum E layer signal with a base tuning susceptance of zero and minimum F layer signal with 3.0 mmhos.

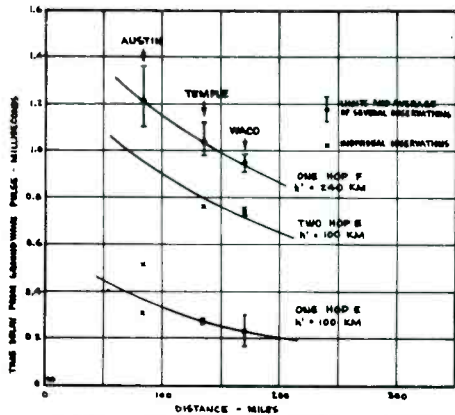


FIGURE 16. RESULTS OF PULSE DELAY MEASUREMENTS

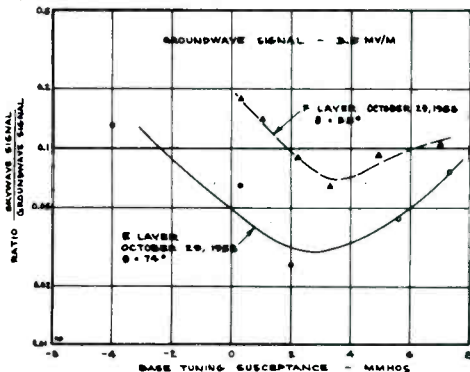


FIGURE 17. RESULTS OF AMPLITUDE ANALYSIS OF PULSE MEASUREMENTS AUSTIN - 64 MILES

Figure 20 shows the relation between base tuning susceptance and the vertical angle of minimum radiation as deduced from the data shown by Figures 17, 18, and 19. The angle of minimum radiation may be varied from  $38^\circ$  to  $74^\circ$  by varying the base tuning. The final tuning selected provides minimum vertical radiation at an angle of approximately  $42^\circ$ .

The strong F layer skywave signals observed on the nights of October 28 and October 29 indicate that F layer transmission may be an important factor in the design of anti-fade antennas for use in the higher frequency portion of the

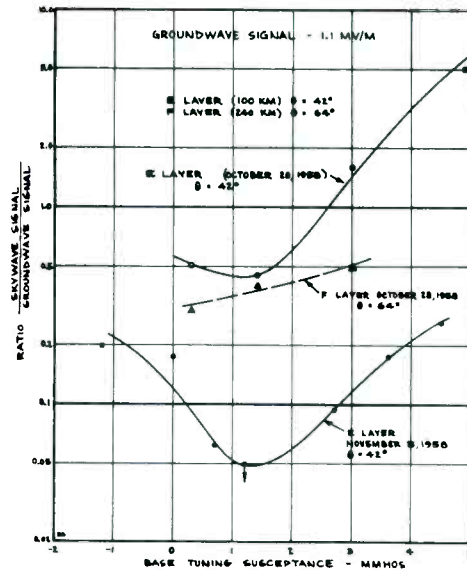


FIGURE 18. RESULTS OF AMPLITUDE ANALYSIS OF PULSE MEASUREMENTS - TEMPLE - 136 MILES

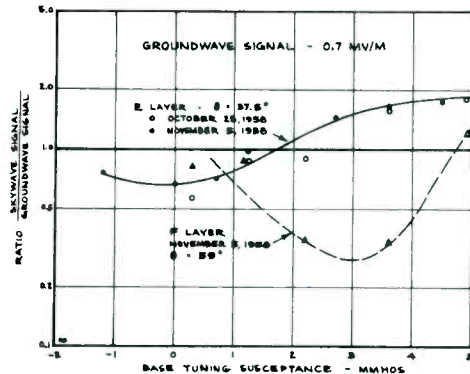


FIGURE 19. RESULTS OF AMPLITUDE ANALYSIS OF PULSE MEASUREMENTS - WACO - 170 MILES

broadcast band. The presence of F layer signals has also been reported by DeWitt and Ring,<sup>11</sup> who made measurements at a frequency of 1410 kc. The observations made at Austin on the night of October 29 show that the signal completely penetrated the E layer except toward daybreak when weak E layer signals were observed. Time was not available to make further pulse observations to establish whether the F layer transmission observed on

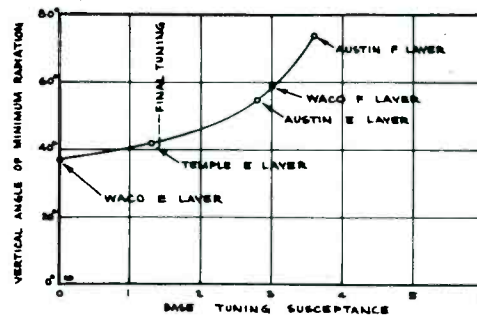


FIGURE 20. EFFECT OF BASE TUNING ON ANGLE OF MINIMUM RADIATION

October 28 was an isolated instance or occurred for an appreciable percentage of the time. The results obtained clearly indicate the need for obtaining more measurements of this type so that the mechanics of skywave propagation for this frequency range will be more fully understood.

Figure 21 shows the current distribution measured on the full scale antenna with the final base tuning adjustment. A movable sampling loop was connected to one of the regular sampling lines so that amplitude and phase measurements could be made by employing the phase monitor at the base of the antenna. The sampling loop was spaced several feet from the center of the tower to minimize pick-up from stub currents. It can be seen that the current distribution obtained on the full scale antenna closely approximates the current distribution shown by the dashed lines as obtained on the model with no capacity stub.

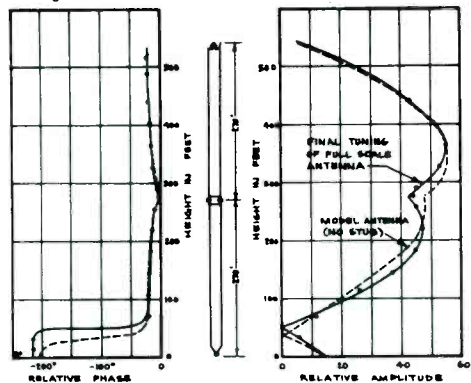


FIGURE 21. CURRENT DISTRIBUTION MEASUREMENTS FOR FINAL TUNING - ( $b = 1.4$  mms)

Figure 22 shows the vertical radiation pattern for the final tuning of the antenna compared with the vertical pattern obtained for the model with no capacity stub. The vertical patterns were computed from the current distribution measurements by a mechanical integration process. Further integration of the vertical pattern for the full scale antenna indicates a no loss inverse field strength at one mile of 1950 mv/m for a power of 50 kw.

Figure 23 shows the groundwave and skywave signals for the final adjustment of the antenna as compared with the originally intended tuning of the

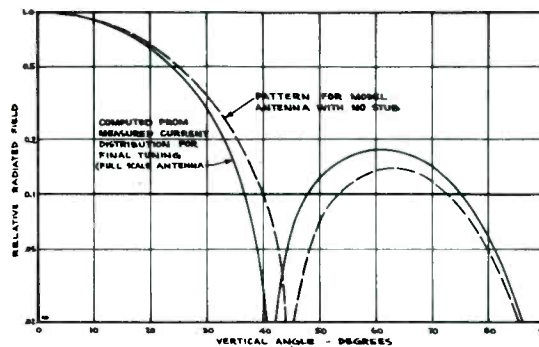


FIGURE 22. VERTICAL RADIATION PATTERN FOR FINAL TUNING ( $b = 1.4$  mms)

antenna. The measured groundwave signal on the route through Austin and Temple is also shown, and it is evident that the measured groundwave field strength was considerably higher than predicted. In view of the higher than expected groundwave signal, it was decided to select the final tuning condition shown rather than the tuning condition which would most closely approximate the originally intended performance. The final tuning provides minimum radiation at a vertical angle of approximately  $42^\circ$ , which corresponds to a distance of 150 miles for E layer transmission. Skywave signals computed for an F layer virtual height of 240 km are also shown by Figure 23. Further observations, including field strength measurements to establish the limit of groundwave service in several directions, are now being made to determine whether any change in tuning may be desirable.

Radial groundwave field strength measurements were made in 8 radial directions to establish the efficiency of the WOAI antenna. The RMS inverse field

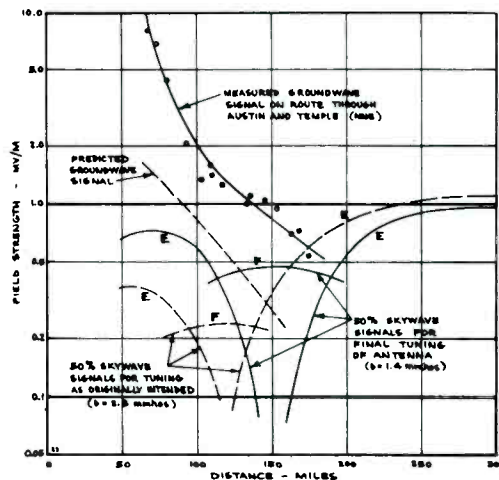


FIGURE 23. GROUNDWAVE AND SKYWAVE SIGNALS FOR FINAL AND ORIGINALLY INTENDED TUNING OF ANTENNA

at one mile was found to be approximately 1890 mv/m. This value is in good agreement with the expected values of 1845 mv/m based on the original design pattern and 1950 mv/m obtained by integration of the radiation pattern as based on the current distribution measurements.

The antenna input impedance at the sectionalizing level for the final base tuning was measured to be  $110 + j 200$  ohms. The impedance value was determined by measuring the input impedance at the lower end of the transmission line with the output end connected directly across the sectionalizing insulators. The impedance was then transferred to the output end of the line by means of a Smith chart.

The authors wish to acknowledge the considerable help provided by A. D. Ring who actively participated in establishing the design criteria and selecting the optimum radiation pattern.

#### CONCLUSION

The design of an anti-fade antenna for broadcasting purposes requires careful consideration of all pertinent factors, including the frequency of operation and the ground conductivity. A rapid build-up of skywave signal just beyond the primary service area is required to minimize the rapid fading zone. For best results the design should incorporate a range of control of the vertical radiation pattern. The effect of practical current distributions on the vertical radiation patterns must be considered. Measurements on a model of the proposed antenna performance form a good basis for making a final evaluation of the performance before constructing the full scale antenna.

After the actual antenna has been constructed, careful measurements are required to insure that the optimum performance is obtained. The suppression of skywave signals may be checked by employing pulse transmissions, and limited measurements indicate that F layer transmissions are sometimes predominant. Finally, the current distribution (both amplitude and phase) of the full scale antenna should be measured and the vertical radiation pattern computed from the current distribution data.

#### REFERENCES

1. G.H. Brown, "A Critical Study of the Characteristics of Broadcast Antennas as Affected by Antenna Current Distribution," Proc. I.R.E., Vol. 24, pp. 48-81, Jan., 1948.
2. H. Page, "Anti-Fading Series-Loaded Mast Radiators," B.B.C. Quarterly Vol. 2, pp. 165-176, Oct., 1947
3. C. L. Jeffers, "An Antenna for Controlling the Non-fading Range of Broadcasting Station," Proc. I.R.E., Vol. 36, pp. 1426-1431, Nov., 1948
4. H. Brueckmann, "Anti-fading Broadcast Antenna," Electronics, Vol. 23, pp. 82-85, May, 1950
5. J. D. Tillman, W. T. Patton, C. E. Blakely, and F. V. Schultz, "The Use of a Ring Array as a Skip Range Antenna," Proc. I.R.E., Vol. 43, pp. 1655-1660, Nov., 1954
6. H. Page and G. D. Monteath, "The Vertical Radiation Patterns of Medium-Wave Broadcasting Aerials," Proc. I.E.E. Part B, Vol. 102, pp. 279-297, May, 1955
7. S. A. Schelkunoff and H. T. Friis, "Antennas, Theory and Practice," John Wiley and Sons, Inc., New York, 1952.
8. R. King and D. Middleton, "The Cylindrical Antenna, Current and Impedance," Quart. Appl. Math., Vol. III, pp. 302-339, Jan., 1946
9. T. Morita, "Current Distributions on Transmitting and Receiving Antennas," Proc. I.R.E., Vol. 38, pp. 898-904, Aug., 1950
10. B. Storm, "Cylindrical Aerials," Wireless Engineer, Vol. 29, pp. 174-176, July, 1952
11. J. H. DeWitt and A. D. Ring, "Significant Radiation from Directional Antennas of Broadcast Stations for Determining Skywave Interference at Short Distances," Proc. I.R.E., Vol. 32, pp. 668-673, Nov., 1944

APPENDIX

METHOD OF DETERMINING CURRENT  
DISTRIBUTIONS AND VERTICAL RADIATION  
PATTERNS OF CYLINDRICAL RADIATORS

A. Conventional Radiators (Power  
Applied at Base)

Schelkunoff and Friis<sup>7</sup> have shown a method for determining the current distribution on a cylindrical radiator of a given diameter where the length is such as to make the radiator anti-resonant. In the case of a radiator above a ground plane, the anti-resonant length is defined as the length (near  $\lambda/2$ ) where the base input reactance is zero and the resistance is at or near the maximum value. For our purpose the equation for current distribution given by Schelkunoff and Friis has been rearranged so as to permit an extension to radiators of other lengths.

The current may be expressed as:

$$I_z = I'_z - j I''_z \quad (1)$$

$$I'_z = \frac{I'_{\max}}{2} [1 - \cos \gamma (G_o - z)] \quad (2)$$

$$I''_z = I''_{\max} \sin \gamma (G_o - z) \quad (3)$$

where:

$I_z$  = current at height  $z$ ,

$z$  = height in degrees above ground plane,

$I'_z$  = real or "in-phase" component of current,

$I''_z$  = imaginary or quadrature component of current,

$I'_{\max}$  and  $I''_{\max}$  = maximum values of  $I'_z$  and  $I''_z$

$v = \frac{c}{v}$  or the ratio of the velocity of light to the phase velocity of the antenna,

and  $G_o$  = overall height of radiator.

For an antenna of anti-resonant length the current at  $z = 0$  is equal to  $I'_{\max}$ , thus

$$I'_{\max} = \sqrt{\frac{P}{R_o}} \quad (4)$$

where  $P$  is the power and  $R_o$  is the base input resistance of the anti-resonant length radiator.

The value of  $\gamma$  can then be determined from

$$\gamma = \frac{180}{l_o} \quad (5)$$

where  $l_o$  is the length of the anti-resonant radiator in degrees. Appropriate values of  $R_o$  and  $l_o$  may be determined from graphs or equations given by Schelkunoff<sup>7</sup> or others.<sup>8,9,10</sup>

The value of  $I''_{\max}$  is determined so as to satisfy the required relationship between current and groundwave efficiency for a given power input. For the current distribution of equations 1 - 3 and assuming anti-resonant length ( $\gamma G_o = 180^\circ$ ) it can be shown that:

$$E_o = 0.651 G_o \sqrt{(I'_{\text{avg}})^2 + (I''_{\text{avg}})^2} \quad (6)$$

$$I'_{\text{avg}} = \frac{I'_{\max}}{2} \quad (7)$$

$$I''_{\text{avg}} = \frac{2 I''_{\max}}{\pi} \quad (8)$$

Where  $E_o$  is the inverse field strength in mv/m, at a distance of one mile along the ground plane, and  $I'_{\text{avg}}$  and  $I''_{\text{avg}}$  are the respective average currents in amperes along the radiator. It follows that  $I''_{\max}$  is given by

$$I''_{\max} = \frac{\pi}{2} \sqrt{\left(\frac{E_o}{.651 G_o}\right)^2 + \left(\frac{I'_{\max}}{2}\right)^2} \quad (9)$$

The value of  $E_o$  to be used in equation (9) may be taken from data given by Brown<sup>1</sup>, which shows the ground plane radiation efficiency of vertical radiators with reduced velocity, sinusoidal current distribution. This approximate method of determining  $E_o$  amounts to neglecting the influence of the  $I'$  component of current on the radiation efficiency of the antenna. It can be shown, however, that this method yields

results which are quite accurate for the range of effective radiator diameters generally in use for standard broadcast station antennas.

For radiators of other than anti-resonant length an approximate current distribution may be obtained from

$$I_z/k_o = \frac{k_1}{2} [1 - \cos \gamma (G_o - z)] - j \sin \gamma (G_o - z) \quad (10)$$

Where  $k_o$  is a constant to relate the absolute current to the relative current distribution and  $k_1 = I'_{\max}/I''_{\max}$ . The values of  $I'_{\max}$ ,  $I''_{\max}$  and  $\gamma$  are based on the solution for a radiator of anti-resonant length and the given effective diameter. This method yielded current distributions A and B shown by Figure 3. The results appear to be reasonable as long as the length of the radiator is not much greater than the anti-resonant length.

The vertical radiation patterns for non-sectionalized radiators such as A and B of Figure 3 were computed by the usual integration of the current distribution:

$$f(\theta) = \frac{\cos \theta \int_0^{G_o} I_z \cos(z \sin \theta) dz}{\int_0^{G_o} I_z dz} \quad (11)$$

where  $f(\theta)$  is the vertical radiation at angle  $\theta$  above the ground plane, normalized with respect to the ground plane radiation.

Solution of this integral expression yields

$f(\theta) = N/D$  where:

$$N = \frac{2\gamma \cos \theta}{\gamma^2 - \sin^2 \theta} [\cos \gamma G_o - \cos S_o] - j k_1 \cos \theta \left\{ \frac{\sin S_o}{\sin \theta} + \frac{\gamma}{\gamma^2 - \sin^2 \theta} \left[ \frac{\sin \theta \sin S_o}{\gamma} \sin \gamma G_o \right] \right\}$$

$$D = \frac{2}{\gamma} (\cos \gamma G_o - 1) - j k_1 \left( \frac{G_o}{57.3} - \frac{\sin \gamma G_o}{\gamma} \right) \quad (12)$$

and where:  $S_o = G_o \sin \theta$

#### B. Sectionalized Radiators with Current Distribution Symmetrical about Sectionalizing Insulator.

The current distribution shown for radiator C of Fig. 3 is based on a radiator sectionalized at the midpoint with the current distribution assumed to be symmetrical about the feed point. The approximate current distribution for a sectionalized radiator with the current symmetrical about the feed point may be expressed by dividing the radiator into lower and upper sections of lengths  $G_1$  and  $G_2$  respectively.

For the lower section

$$\frac{I_{1z}}{k_o} = \frac{k_1}{2} [1 - \cos \gamma (G_2 - G_1 + z)] - j \sin \gamma (G_2 - G_1 + z) \quad (13)$$

and for the upper section

$$\frac{I_{2z}}{k_o} = \frac{k_1}{2} [1 - \cos \gamma (G_o - z)] - j \sin \gamma (G_o - z) \quad (14)$$

As before the constants  $k_1$  and  $\gamma$  were determined from the solution for a radiator of anti-resonant length.

The integration of the current distribution expressed by equations (13) and (14) may be performed in parts to yield

$f(\theta) = N/D$  where

$$N = \frac{2\gamma \cos \theta}{\gamma^2 - \sin^2 \theta} [2 \cos \gamma G_2 \cos S_1 - \cos \gamma(G_2 - G_1) - \cos S_0] - jk_1 \cos \theta \left\{ \frac{\sin S_0}{\sin \theta} + \frac{\gamma}{\gamma^2 - \sin^2 \theta} [\sin \gamma (G_2 - G_1) - 2 \sin \gamma G_2 \cos S_1 + \frac{\sin \theta \sin S_0}{\gamma}] \right\}$$

$$D = \frac{2}{\gamma} [2 \cos \gamma G_2 - \cos \gamma(G_2 - G_1) - 1] - jk_1 \left[ \frac{G_0}{57.3} - \frac{1}{\gamma} [\sin \gamma(G_2 - G_1) - 2 \sin \gamma - G_2] \right] \quad (15)$$

where  $S_n = G_n \sin \theta$

C. Sectionalized Radiator with Power Applied Both at the Base and at the Sectionalizing Level.

The current distribution for a modified Jeffers antenna as shown for radiator D of Figure 3 was predicted by combining two current distributions predicted by the methods outlined above. Current Components  $I_A'$  and  $I_A''$  represent a symmetrical distribution about the upper feed point as determined from equations (13) and (14). Current components  $I_B'$  and  $I_B''$  represent the expected current distribution on the lower section due to the power applied at the base as determined from equation (10). The total current is simply the sum of the A and B

components with the ratio adjusted to produce the desired loop current ratio. The length of the upper section was made equal to the anti-resonant length in order to simplify this simulation of the current distribution.

The vertical radiation pattern for the modified Jeffers antenna was computed by adding the two radiation patterns produced by the two sets of current components with appropriate constants inserted to maintain the proper relative magnitude of the two patterns. The individual patterns were determined from equations (12) and (15).

D. Evaluating the Equivalent Cylindrical Cross Section of a Tower with Uniform Cross Section.

The equivalent cylindrical diameter of a tower may be determined by computing the effective cylindrical diameter of the three tower legs. Generally the effect of cross and diagonal bracing members may be neglected. Schelkunoff and Friis<sup>7</sup> have shown that

$$a_{\text{eff}} = a \left( \frac{n a_0}{a} \right)^{1/n} \quad (16)$$

Where  $a_{\text{eff}}$  = radius of equivalent cylinder.

- $A_0$  = radius of tower legs
- $n$  = number of tower legs
- $a$  = distance from center of tower legs to center of tower cross section.